Spectrochimica Acta Part B 90 (2013) 1–22

Contents lists available at ScienceDirect

Spectrochimica Acta Part B

journal homepage: www.elsevier.com/locate/sab

Review

Thermodynamic equilibrium states in laser-induced plasmas: From the general case to laser-induced breakdown spectroscopy plasmas

G. Cristoforetti *, E. Tognoni, L.A. Gizzi

National Institute of Optics (INO) of the National Research Council (CNR), Via G. Moruzzi 1, 56124 Pisa, Italy

ARTICLE INFO

Article history:
Received 26 June 2013
Accepted 23 September 2013
Available online 1 October 2013

Keywords:
Laser-induced plasma
Local thermodynamic equilibrium
Recombination
Ionization
LIBS

ABSTRACT

Applications, present and potential, of laser-induced plasmas are today widespread in a large range of fields and continue to extend each day because of the advancement of laser science and technology. These circumstances call for a better knowledge and characterization of physical and chemical processes occurring in a plasma. The spectrum of the radiation emitted by the plasmas is a mine of information about the plasma state and therefore spectroscopy remains one of the key techniques for its investigation. The interpretation of emission spectra, however, requires a deep knowledge of the elementary processes determining the atomic state population and the fractional ion densities, and of their balance. The transient character of laser-induced plasmas and the presence of spatial gradients introduce time-dependent and non-local effects in the energy level population, and thus increase the complexity of the plasma modeling. The thermodynamic approach, describing the atomic and ionic state population by statistical distributions, is the easiest and the most widely used way to model the plasma state but does not account for non-local and non-steady-state effects. It is therefore in many cases unfit for this purpose. As a consequence, kinetic modeling of the plasma is often needed, which must be in many cases integrated by hydrodynamic modeling of plasma expansion and appropriate equations describing the transport of radiation and charged particles into the plasma.

In this complex framework, this paper aims at giving a concise description of theoretical issues, redirecting to the key literature for more details, and to delineate possible scenarios occurring in the wide range of laser-induced plasmas. Examples of different classes of laser-induced plasmas are reported, including some experimental results for completeness. Special attention is devoted to the case of 'cold' or thermal plasmas, in particular those produced in laser-induced breakdown spectroscopy. The occurrence of local thermodynamic equilibrium is, in that case, discussed as well as the relevance of phenomena leading the system out of equilibrium, such as radiative, transient and diffusive processes. The most important directions for future work, in particular regarding non-stationary and diffusive effects, are also suggested.

Contents

Abbreviations: ASDF, atomic state distribution function; CE, coronal equilibrium; CF-LIBS, calibration-free laser-induced breakdown spectroscopy; CR, collisional–radiative; CRE, collisional–radiative equilibrium; CRC, capture-radiative cascade; CTE, complete thermodynamic equilibrium; DSB, deexcitation saturation balance; EEDF, electron energy distribution function; EEK, electron excitation kinetic; ESB, excitation saturation balance; HEDF, heavy particle energy distribution function; IB, ionization balance; ICP, inductively-coupled plasma; LIBS, laser-induced breakdown spectroscopy; LIP, laser-induced plasma; LTE, local thermodynamic equilibrium; PLTE, partial local thermodynamic equilibrium; SW, shock wave.

* Corresponding author. Tel.: +39 050 3152222; fax: +39 050 315 2247.
E-mail address: gabriele.cristoforetti@cnr.it (G. Cristoforetti).

0584-8547/$ – see front matter © 2013 Elsevier B.V. All rights reserved.
http://dx.doi.org/10.1016/j.sab.2013.09.004

1. Introduction

The interest in modeling the dynamic and thermodynamic evolutions of laser-induced plasmas (LIP) has exponentially grown in the last fifty years, because of the impressive number of applications they have or potentially could provide in the future, going from the medical therapy to the chemical analysis of materials, from the production of X-ray or energetic particles to the micro/nano-structuring of surfaces, from the research toward nuclear fusion to the astrophysical investigation. The rapid progress in laser technology provides laser pulses increasingly short and energetic every day, allowing plasmas hotter and denser to be investigated, challenging experimental research and modeling.

Among the experimental techniques, which are commonly used to investigate laser plasmas, spectroscopy is definitely and historically of paramount importance, because it provides access to a wealth of information about the plasma state. The intensity of the emission lines, in fact, is strictly correlated with the population distribution among the atomic energy levels (atomic state distribution function, ASDF) and among the ionization stages (often referred as charge state distribution or fractional ion density distribution). At the same time, the intensity and the spectral distribution of the continuum emission provide information about the kinetic energy distribution of the electrons (electron energy distribution function, EEDF). Thus, a correct interpretation of the emission spectrum provides an insight into the balance of the elementary processes populating and depopulating the excited levels, the ionization stages and the electron energy states. In the most favorable case, where thermal equilibria between atomic energy levels and between electron kinetic energies hold, i.e. ASDF and EEDF can be described by Boltzmann and Maxwell distributions, respectively, the spectrum inspection allows the temperature of the plasma to be calculated. In particular cases, the emission spectrum allows one also to derive information about the kinetic energy distribution of atoms/ions (heavy particle energy distribution function, HEDF) and, if Maxwell equilibrium is established between them, their temperature can be calculated.

In order to give a correct interpretation of plasma spectra it is necessary to know what is the thermodynamic state of the plasma, i.e. the balance established between the elementary processes determining the population of energy states. In other words, it is necessary to know the relative importance of collisional excitation/de-excitation processes, ionization by collisions, photoionization, radiative and three-body recombination, radiative decay, photoexcitation and Bremsstrahlung processes, dielectronic recombination and autoionization. In this view, we delineate some extreme ideal cases that can represent a reference point for the orientation of the spectroscopist.

The easiest situation to depict is that of a plasma stationary and homogenous, i.e. a plasma where the population of energy states does not change in time and in space, and is not affected by the diffusion/transport of particles. Such a situation is evidently not reproducible in the laboratory; however, this case applies to all the plasmas where the temporal variation of thermodynamic parameters is sufficiently slow and the inhomogeneity effects are negligible. In this case, no deviations from ionization balance (hereafter IB) are produced, which means that ionization and recombination rates are the same. Moreover, the population among translational (EEDF and HEDF) and internal energy levels (ASDF) is uniquely determined by the values of electron density n_e and electron temperature T_e. Such values, in fact, fix the rates of all the elementary processes producing excitation/deexcitation and ionization/recombination in the ensemble of ions and electrons. In the general case, by using a collisional–radiative (CR) model, according to the scheme proposed by Bates et al. [1,2], the population of the energy states can be numerically or analytically calculated by solving a complex system of rate equations, which accounts for the occurring elementary processes and for their respective reaction rates. The treatment of opacity would need the integration of the CR model with a radiation transport model which intrinsically produces non-local effects; however, such a problem is usually skipped by introducing an escape factor in the line emissivity, which results in an effective reduced probability of spontaneous radiative decay. A much easier approach to describe the population of atoms and ions in stationary/homogenous plasmas can be however used under particular conditions, for example when all the elementary processes are in equilibrium,[1] i.e. the direct and inverse rates of the process are the same, as in complete thermodynamic equilibrium, CTE, or, otherwise, when the rate of some of these processes is low enough to be safely neglected, as for example in the cases of Local Thermal Equilibrium (LTE) and coronal equilibrium (CE). While CTE can be approximately realized in laboratory plasmas only in carefully designed experiments (e.g. in cavities hohlraums), because radiation usually escapes from the plasma and is therefore decoupled from particles, CE and LTE represent a sufficiently accurate description for plasmas in particular situations, when the density of electrons is sufficiently low or high, respectively.

The scheme outlined above is the most utilized in the literature, where often the existence of CE or LTE is checked by simply comparing the measured electron density to the corresponding theoretical thresholds. Actually, such approach is too naïve in many practical cases, since a laser-induced plasma is neither stationary nor homogenous. The transient character of LIPs and the presence of spatial gradients can produce important effects in the balance of the elementary processes and lead to significantly different population balances between the energetic levels.

Accounting for the transient nature of the plasma can be a hard task, since in that case the plasma modeling is strictly related to its dynamic evolution, which includes the early stage of plasma formation and the late stage of plasma expansion and cooling, where in both the stages the IB is violated. In the former stage, occurring during the laser pulse, the radiative energy absorbed by the plasma produces a rapid excitation and ionization of atoms, so that the plasma is ionizing (i.e. ionization rate is higher than recombination rate). In the latter, both the energy lost via radiative emission, electron diffusion and interaction with the background gas, and the conversion of internal energy into translation energy occurring during the expansion of the plasma plume,[2] produce a deexcitation of energy levels and ion recombination, so that the plasma is recombining.

[1] In this paper the expressions 'thermodynamic equilibrium' and 'thermal equilibrium' are used interchangeably.

[2] In the context of laser-induced plasmas, the term 'plume' indicates the volume containing the ablation products.

Similarly, deviations from the IB can be produced by plasma inhomogeneity, due to an inward/outward spatial flux of ions or neutral atoms due to particle diffusion.

In both the cases of transient and inhomogeneous plasmas, retrieving the population distribution of an atomic/ionic ensemble can be obtained by utilizing a CR code in conjunction with simulations by a hydrodynamic plasma code. Alternatively, experimental data describing plasma temporal and spatial evolutions can be considered in place of simulations. In these cases, it is crucial to establish how rapidly the temporal and spatial effects produce variations in the free electron and ion density. If changes are sufficiently slow, the atomic system has enough time to relax to its new equilibrium and thus evolves through successive quasi steady states. In this case, which is not practically different from the stationary state case described before, a CR model can be easily applied to describe the ASDF at each time and position, provided that local and time-resolved values of electron density and temperature are known.

The situation, however, becomes much more complex if the variation in electron and ion density produced by transient and inhomogeneity nature of the plasma is faster than the typical relaxation of the system to the equilibrium. In this case, the population of energy levels at a certain time and position depends not only on the local values of the electron density and temperature at that time, but also on the *history* of plasma evolution up to that time. To describe such systems it is necessary to use a time-dependent CR model, coupled to a hydrodynamic code and to an accurate guess of the initial conditions of the problem.

A satisfactorily treatment of plasma spatial gradients, i.e. of inhomogeneous plasmas, requires a model for the diffusion/transport of particles and a non-local treatment of radiation using a radiation transport code.

Plasmas belonging to these categories are therefore the most difficult to describe because an accurate picture of their thermodynamic state is strictly related to the modeling of the plasma dynamical evolution and of the non-local effects and needs a sufficiently accurate knowledge of the initial conditions of the atomic energy system. Depending on the time- and space-evolution, such plasmas can be far from IB and, in some cases, they can never reach CE or LTE conditions, even for extremely low or high electron density values. Differently, depending on the values of electron density and electron temperature, other types of balances can be reached, as for example ladder-like Excitation Saturation Balance (ESB) in case of ionizing plasmas and Capture Radiative Cascade (CRC) or ladder-like Deexcitation Saturation Balance (DSB) in case of recombining plasmas [3].

In the experimental practice, the thermodynamic state of a LIP (i.e. the type of balance determining the ASDF and the charge state distribution) mainly depends on the laser irradiance and its temporal evolution, on the gas/vacuum environment, on the target/plasma composition and finally on the stage of evolution considered. Given its intrinsic transient nature, a laser-induced plasma necessarily undergoes a phase of strong ionization during laser irradiation and a recombination phase during plume expansion and cooling. Depending on the experimental conditions, many types of balance can occur in laser-induced plasmas, as shown in the wide literature affording the issue. Here we delineate possible scenarios occurring in LIP, focusing in particular on situations where LTE is approached. Because of the multitude of situations that can occur, after a schematic theoretical description of different scenarios and after presenting different examples in several classes of plasmas, we will focus here on the special case of plasmas typical of laser-induced breakdown spectroscopy (LIBS), i.e. 'cold' plasmas (temperatures in the range 0.5–5 eV in the typical observation window) induced by laser irradiances in the range 10^8–10^{12} W cm^{-2}. Particular attention will be given to the issue of plume expansion, which is often neglected in many papers assuming LTE, and to the role played by gas environment in determining plasma cooling time. A review of the main papers discussing theoretically or experimentally the problem of LTE occurrence in LIBS plasmas will also be given.

2. Theoretical

In this chapter we give a schematic and concise theoretical framework of both the elementary processes determining quantum state population and different types of balances among them. Clearly, the presentation cannot be exhaustive of all possible situations, because of the multitude of processes involved. The reader can find a more detailed and analytical picture in Fujimoto [4] and van der Mullen [5].

2.1. Electron excitation kinetic plasmas

We will focus our attention to electron excitation kinetic (EEK) plasmas, where the transitions between energy states are ruled by collisions with electrons rather than with heavy particles. When electrons and ions have a similar temperature ($T_e \approx T_H$), the rates of collision among electrons (ν_{ee}), among ions (ν_{HH}) and between electrons and ions (ν_{eH}) obey the relations $\nu_{HH} \sim (m_e/m_H)^{1/2}\nu_{ee}$ and $\nu_{eH} \sim (m_e/m_H)\nu_{ee}$. This implies that the energy exchange between electrons (bound and free) is much more effective than that between ions and electrons. Considering the above scaling laws, in laser-induced plasmas, where usually the ion temperature T_H is less than, or of the order of, the electron temperature T_e, even a small ionization degree of the order of $\approx 10^{-4}$ is sufficient to ensure that electron collisions are dominant. Therefore, the great majority of LIPs, which have a larger ionization degree, can be safely included in this class. The cases where $T_H > T_e$ need a more complex approach and are not discussed here.

Due to the large collisional rate between electrons, in EEK plasmas free electrons rapidly reach thermal equilibrium so that the bulk of EEDF is described by a Maxwell distribution. The electron–electron relaxation time $\tau_{rel}^{e,e} \approx 1/\nu_{ee}$, expressed in seconds, can be calculated by the Spitzer formula [6],

$$\tau_{rel}^{e,e} \approx \frac{3.3 \cdot 10^5 (kT_e)^{3/2}}{n_e \ln \Lambda} \tag{1}$$

where kT_e is the electron temperature in eV, n_e the electron density in cm^{-3} and lnΛ is the Coulomb logarithm [6,7], slowly varying with n_e and T_e, whose value in LIPs is typically of the order of 10. Considering the abovementioned scaling laws of the collisional rates (at $T_e \approx T_H$), the relaxation time of ions to a Maxwellian distribution, $\tau_{rel}^{HH} \approx 1/\nu_{HH}$, and the thermalization time between electrons and ions, $\tau_{rel}^{eH} \approx 1/\nu_{eH}$, are larger by a factor of $(m_H/m_e)^{1/2}$and (m_H/m_e), respectively.

The escape of radiation from the plasma as well as deviations of ASDF from Boltzmann distribution can produce improper balances of inelastic and superelastic collisions and then a distortion in the high energy tail of the Maxwellian velocity distribution of the electrons, as shown for example in Refs. [8–10]. Other possible causes of deviation from a Maxwellian distribution are non-linear plasma processes, as for example plasma instabilities or collisionless absorption mechanisms of laser energy. These cases are increasingly important at larger laser irradiance values (approximately > 10^{14} W cm^{-2}), where the collisional absorption of laser energy (i.e. via inverse Bremsstrahlung process) becomes ineffective, and are briefly mentioned in Section 3 for the sake of completeness. The bulk of the electrons retains however a thermal equilibrium due to the effectiveness of energy exchange in distant encounters, so that an EEK plasma can be considered as an ensemble of atoms and ions immersed in a "Maxwell bath". For this reason, in the paper we refer to electron temperature T_e, i.e. that is expressed in the Maxwell distribution, also in the cases where the population of the atomic/ionic levels is not in thermodynamic equilibrium. The description of relativistic plasmas, where the electron kinetic energy is comparable to its rest mass and where EEDF deviates significantly from a Maxwell distribution, is not in the scope of this paper.

2.2. The collisional–radiative model

To describe the different thermodynamic states which can occur in EEK plasmas, it is useful to recall the basic ideas underlying the CR model, as introduced by Bates et al. [1,2]. According to the CR model, it is possible to describe the population $n_Z(p)$ of an excited level p of the ion Z as the sum of two components, one deriving from the direct excitation of the ground population $n_Z(1)$ (hereafter the ground level), and the other from deexcitation and recombination processes starting from the population of the ground level n_{Z+1} of the next ion stage[3] (hereafter the ion level). Obviously, in cases where neutral atoms and singly-charged ions are present in the plasma, as for example in LIBS case, n_Z and n_{Z+1} refer to the population of neutral and ions, respectively. On this basis, the departure $b(p)$ of the population $n_Z(p)$ from the Saha–Boltzmann equilibrium population, $n_{Z,SB}(p)$, can be expressed by

$$b(p) = \frac{n_Z(p)}{n_{Z,SB}(p)} = r_0(p) + r_1(p)b(1) \tag{2}$$

where $r_0(p)$ and $r_1(p)$ are named respectively the recombining and the ionizing coefficients. The parameters $r_0(p)$ and $r_1(p)$ are related to the processes of deexcitation and recombination from the ion level and to those of excitation from the ground state, respectively, and to their reaction rate and depend on electron density and electron temperature [4].

In this scheme ground and ion levels can be viewed as sources of electrons, whose population is sufficiently large not to be affected by the electron flux populating the excited levels. Moreover, since the relaxation time of ground and ion levels is much larger than that of the excited levels, their population can be considered fixed during the time the excited levels reach the equilibrium. In conclusion, the population of excited levels can easily be calculated whenever ground and ion populations and $r_0(p)$ and $r_1(p)$ – i.e. n_e and T_e – are known, by solving a set of linear equations of the type reported in Eq. (2).

Determining the populations of the ground and ion levels can then be considered a decoupled problem. They change on times much longer than relaxation times of excited levels and are strongly affected by slow processes, besides ionization and recombination, as ambipolar diffusion, plasma expansion and plasma cooling. The rate of variation of $n_Z(1)$ and n_{Z+1} can be expressed by the continuity equations [5]

$$\frac{\partial n_Z(1)}{\partial t} = -\tilde{\nabla}\cdot n_Z(1)w_1 + n_e n_{Z+1}\alpha_{CR} - n_e n_Z(1)S_{CR} \tag{3a}$$

$$\frac{\partial n_{Z+1}}{\partial t} = -\tilde{\nabla}\cdot n_{Z+1}w_+ - n_e n_{Z+1}\alpha_{CR} + n_e n_Z(1)S_{CR}. \tag{3b}$$

Here w_1 and w_+ have the dimensions of a velocity, the divergence terms represent a flow (sink or source) of $n_Z(1)$ and n_{Z+1} populations and account for the diffusion of particles and for the expansion of the plume; α_{CR} and S_{CR} are the total coefficients of recombination and ionization. It should be noted here that in non-hydrogenic systems, metastable levels are often present, which have relaxation times much longer than those of excited levels and of the same order of that of the ground and ion levels. Therefore, in the CR formulation, metastable levels should be considered at this stage and appropriate continuity equations should be considered for them, to be included in the system of equations expressed in Eqs. (3a) and (3b). The second term on the right hand side (r.h.s.) accounts for the direct recombination processes to the ground level plus the deexcitation of that part of population of the excited levels originating from the ion level. The third term on the r.h.s. accounts for the direct excitation from the ground level subtracted by the population that comes back by deexcitation processes. It is worth noting the importance of the first term on the r.h.s. in Eqs. (3a) and (3b), which shows that in LIPs the population of ground and ion levels (and metastable levels) can be strongly affected by the spatial relaxation term $\nabla\cdot nw$. This implies that Eqs. (3a) and (3b) should be solved by closing the system of equations with an analytical or numerical description of hydrodynamic expansion of the plume and of electron/atom diffusion processes. Self-consistently, also the expansion of the plume is affected by ionization and recombination flux of the atomic system that subtract or provide thermal energy to the free electrons, respectively, resulting in a slowing down or in an acceleration of the plume.

2.3. Stationary and homogenous plasmas

In stationary and homogeneous plasmas Eqs. (3a) and (3b) reduce to the expression $n_e n_{Z+1}\alpha_{CR} = n_e n_Z(1)S_{CR}$, i.e. the plasma is in IB, and can be rewritten in the form

$$\frac{n_{Z+1}}{n_Z(1)} = \frac{S_{CR}}{\alpha_{CR}} = \frac{S_Z}{\alpha_{Z+1}n_e + D_{Z+1} + \beta_{Z+1}} \tag{4}$$

that gives the fractional density of ions whenever the coefficients of collisional ionization S_Z, three-body recombination α_{Z+1}, dielectronic recombination D_{Z+1} and radiative recombination β_{Z+1} are known.

In the laboratory this situation can apply whenever the plume expansion is sufficiently slow and the spatial gradients sufficiently small, as discussed below in Section 2.5. In this case, the equilibrium balance between energy levels and therefore the ASDF depends on the local and instantaneous values of electron temperature and density in the plasma.

The population of a level p results from the competition between collisional excitation/deexcitation recombination/ionization processes and the radiative decay/recombination processes involving that level. While each collisional process reaches the kinetic equilibrium with its inverse process after a suitable time (i.e. the principle of detailed balance applies in stationary plasmas), this does not occur for radiative processes because LIPs are usually optically thin (at least for most of the wavelengths). Therefore, the imbalance of radiative processes hinders the onset of a Complete Thermal Equilibrium in a LIP, which would require that the principle of detailed balance would apply for all processes. Whenever collisional processes prevail, however, the effect of radiative imbalance on levels population becomes negligible and quantum energy states in the plasma (except those involving radiation states) can be safely described by thermal equilibrium statistics. This type of *proper* balance is named Local Thermal Equilibrium (LTE) and holds for sufficiently high values of the free electron density [11].

According to the original criterion proposed by Griem [12], the prevalence of collisional versus radiative processes on the population of a level p can be expressed by

$$\left[\sum_{q>p} C(p,q) + \sum_{q<p} F(p,q) + S(p)\right] n_e \geq 10\sum_{q<p} A(p,q) \tag{5}$$

where $A(p,q)$, $C(p,q)$ and $F(p,q)$ are the radiative decay probability, the rate of collisional excitation and the rate of collisional deexcitation from level p to level q and $S(p)$ is the ionization rate coefficient. Eq. (5) can be simplified by retaining in the summations only the terms involving the adjacent levels, which are the largest ones, and it finally gives a threshold for the electron density that ensures the prevailing of collisions in determining the population of level p. Similar criteria, allowing to calculate the minimum electron density necessary for keeping two energy levels p and q in local thermodynamic equilibrium have been successively formulated by Drawin [13], Wilson [14], Hey [15] and McWhirter [16]. Eq. (6), already reported in our previous paper [17], accounts for appropriate quantum-mechanical corrections with the

[3] In the CR approach, usually, the population of the ground level of the ion stage $n_{Z+1}(1)$ is considered equal to the total population of the ion n_{Z+1}, since $\sum_{p>1} n_{Z+1}(p) \ll n_{Z+1}(1)$. So, we also use indifferently the symbol n_{Z+1} for both the quantities.

introduction of the thermally-averaged effective Gaunt factor $\langle\overline{g}\rangle$, as obtained from the formulation of Hey [15]

$$n_e > \frac{2.74 \cdot 10^{13}}{\langle\overline{g}\rangle}(kT_e)^{1/2}\left(\Delta E_{pq}\right)^3 \quad (6)$$

where n_e is expressed in cm^{-3} and both kT_e and ΔE_{pq} (the energy gap between levels p and q) are expressed in eV. Approximated values of $\langle\overline{g}\rangle$, obtained by averaging over several species, can be found in Refs. [18,19]. More precise values of the Gaunt factor, obtained theoretically or experimentally for single species, are nowadays available in literature, and can differ even by a factor of two from those reported in Refs. [18,19], especially for complex atomic (ionic) systems. It is worth pointing out that the $\langle\overline{g}\rangle$ values of neutral atoms and ions significantly detach in the low temperature regime (i.e. $\Delta E > kT_e$), which is due to the different values of near-threshold cross-sections for collisional excitation of atoms and ions. This may have profound implications on the LTE validity of cold plasmas, e.g. LIBS plasmas, as discussed in detail in Ref. [20].

Since the rate of collisional excitation (deexcitation), as expressed in Bethe–Born approximation [21], is inversely proportional to ΔE_{pq} and the radiative decay rate increases as $\Delta E_{pq}{}^2$, it follows that the minimum electron density necessary for thermal equilibrium of p and q levels increases as $\Delta E_{pq}{}^3$. This implies that the energy levels that are more easily dominated by collisions with electrons are those near the continuum, where the energy gap between the levels is smaller. Such levels are usually collisionally coupled with upper adjacent levels (Fig. 1b) and therefore are finally in thermodynamic equilibrium with free electrons, whose energy distribution can be considered as a continuum of energy states separated by infinitesimal gaps of energy. Climbing down toward the ground level the importance of radiative decay progressively increases and that of collisions with electrons progressively decreases, so that a level p_G usually exists, called the 'Griem boundary' (or alternatively *the thermal limit* or *the collisional–radiative limit*), for which the collisional rates equal the radiative depopulation rate. The Griem boundary subdivides the atomic level system into two parts where different balances apply, i.e. Partial Local Thermodynamic Equilibrium (PLTE) in the upper part and coronal equilibrium in the lowest end. The Griem boundary climbs down toward lower energy levels when the electron density increases and eventually reaches the ground level when the radiative decay rate from the resonance level is much lower than the collisional excitation rate from the ground level to the first excited level. In this case, the plasma is in local thermodynamic equilibrium. An estimate of the electron density necessary to ensure LTE is usually obtained by substituting the energy of the resonance level ΔE_{21} in Eq. (6). It is important to note that such electron density is also approximately the threshold for which 3-body recombination predominates over radiative recombination [4], so that the fulfillment of Eq. (6) for the ground level ensures also that the ionization balance is in the high density regime.

It is worth recalling some approximations which have been employed above. Firstly, Eq. (6) was derived for allowed transitions, i.e. transitions for which the cross section is given by the dipole term; the treatment of forbidden transitions makes this scheme incorrect and needs an appropriate approach [15]. Secondly, we have completely neglected opacity effects, which can be relevant for the lowest levels of the atomic system; it is now clear from the above considerations that self-absorption of radiation helps the system to reach LTE (it can be considered as a reduction of the effective radiative decay probability). Griem and Drawin [12,13] estimated that the electron density necessary for LTE is lower by about an order of magnitude with respect to that given by Eq. (6), when the resonance transition is optically thick. Finally, we want to note, as remarked by Drawin [13], that in non-hydrogenic atoms, it may happen that the largest energy gap is not that between ground and resonant levels; in this case, the largest gap should be considered for determining the LTE threshold.

In LTE Eq. (2) reduces to $r_0(p) + r_1(p) = 1$, where lower levels are prevailingly populated by excitation from the ground state, i.e. $r_1(p) > r_0(p)$, while higher excited levels are prevailingly populated by collisional deexcitation from the ion state, i.e. $r_0(p) > r_1(p)$. The ASDF is in this case described by the Boltzmann distribution (see Fig. 2) while the ion population is given by the Saha–Eggert relation, which can be easily obtained by Eq. (4) in the high-density limit, by neglecting the radiative and dielectronic recombination terms.

Going to the low-density regime, the radiative decay/recombination processes prevail onto the collisional deexcitation/recombination processes and a different equilibrium balance applies, the coronal equilibrium, which was introduced by Woosley and Allen for modeling the equilibrium of the solar corona [22]. In this case, the population of a level p is given by the balance between collisional excitation from the ground state $C(1,p)$ and the spontaneous emission from that level $\sum_{q<p} A(p,q)$, as depicted in Fig. 1a. This implies that CE is an *improper*

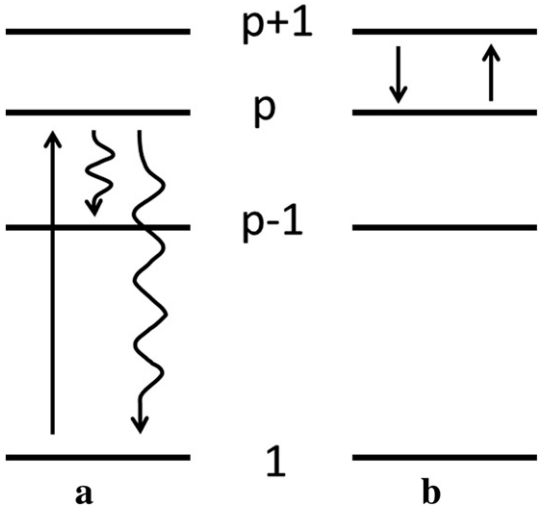

Fig. 1. Two types of equilibrium are illustrated: a) coronal equilibrium; and b) local thermodynamic equilibrium. Straight arrows indicate collisional processes with free electrons, and curved arrows are radiative processes. In (a), we have a balance between collisional excitation and radiative decay, whereas in (b) each collisional process is balanced by its inverse.

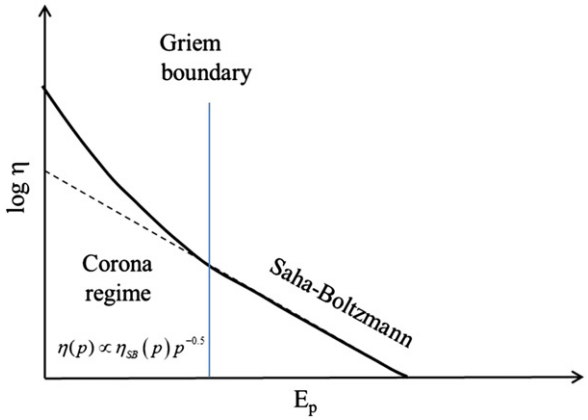

Fig. 2. Boltzmann plot representation of the ASDF for a system in IB, where $\eta(p) = n(p)/g(p)$, $g(p)$ is the degeneracy of the level and E_p is its energy, measured with respect to the ground state. In the coronal equilibrium regime the population expected for a hydrogenic system is also reported where $\eta_{SB}(p)$ is the population predicted in LTE.

balance type, i.e. the principle of detailed balance does not apply. The ASDF is in this case expressed by

$$\frac{n(p)}{n(1)} = \frac{n_e C(1,p)}{\sum_{q<p} A(p,q)} \tag{7}$$

strongly depending on the electron temperature via the collisional excitation cross section $C(1,p)$. Eq. (7) also shows that in CE, the population of the excited levels is proportional to the electron density. The strong radiative decay in the CE results in an overpopulation of lower levels with respect to population predicted by LTE (Fig. 2).

Similarly, collisional ionization is balanced by radiative and dielectronic recombination, so that the ion fractional density can be obtained by neglecting the three-body recombination α_{Z+1} term in Eq. (4). It is now clear from the above considerations that CE is more easily fulfilled by lower energy levels, while it needs lower values of electron density to be verified by the highest levels, which are usually populated by the recombination of ions. CE model can therefore be applied to an atomic system when the electron density is so low that the Griem boundary reaches the ionization level, which can be expressed by the formula of Wilson [14]

$$n_e < 1.5 \cdot 10^{10} \frac{(kT_e)^4}{E_{ion}^{1/2}} \tag{8}$$

where kT_e and the ionization energy E_{ion} are expressed in eV and n_e in cm^{-3}.

The situation in which the electron density is in between the values given by Eqs. (6) and (8) is usually called collisional–radiative equilibrium (CRE). As explained above, in this case, the Griem boundary is located somewhere in the atomic level system and separates the lower part balanced by CE and the upper part balanced by PLTE. The ionic state distribution is obtained by retaining all terms in Eq. (4).

2.4. Ionizing and recombining plasmas

The inspection of balances occurring in ionizing and recombining plasmas is useful to understand the possible deviations of the ASDF and of the charge state distribution from those described in the preceding section, deviations which are due to the transient and inhomogeneous character of a LIP. A plasma is ionizing or recombining according to the value assumed by the expression $n_e n_Z(1) S_{CR} - n_e n_{Z+1} \alpha_{CR}$, higher or lower than zero, respectively, while it is in IB when the expression vanishes.

It is useful to consider the extreme cases of purely ionizing and purely recombining plasmas, where only the term $r_1(p)$ or $r_0(p)$ in Eq. (2), respectively, contributes to the population of the level p. These extreme cases can be representative of the conditions of a LIP during the early stage of plasma formation and during the late stage of plasma cooling, respectively. Balances occurring for different values of T_e and n_e are summarized in Fig. 3 for hydrogen atoms and hydrogenic ions, according to the Fujimoto scheme [4], which can be translated qualitatively to other ionic systems.

We now introduce the Byron boundary p_B [23], which is necessary to understand the balance equilibrium occurring in the high density region, i.e. for $p > p_G$, where collisional processes are dominant. It corresponds to the level p_B for which the collisional depopulation rate $n_e n(p_B) F(p_B, p_B - 1)$ toward the lower adjacent level $p_B - 1$ is equal to the collisional depopulation rate $n_e n(p_B) C(p_B, p_B + 1)$ toward the higher adjacent level $p_B + 1$. Physically, it depends only on the electron temperature and is located roughly in the atomic energy system near the level for which thermal energy kT_e is equal to the energy gap $\Delta E_{pB,pB+1}$. Energy levels located over the Byron limit may be labeled as 'hot' ($kT_e \gg \Delta E_{p,p+1}$) and are depopulated toward higher levels, while those located below may similarly be labeled as 'cold' ($kT_e \ll \Delta E_{p,p+1}$) and are depopulated toward lower levels.

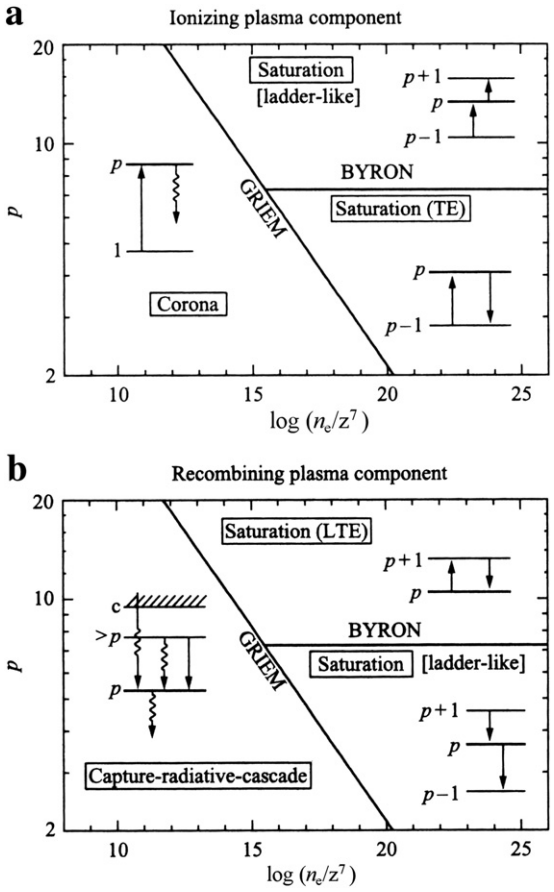

Fig. 3. Summary of balances occurring in hydrogen atoms and hydrogen-like ions in case of purely ionizing (a) and purely recombining plasmas (b), mapped according to Fujimoto's scheme [4]. The lines indicated with labels Griem and Byron represent Griem's and Byron's boundaries. The quantity reported on the abscissa shows that the balances of the system scale as n_e/z^7 where z is the charge of the hydrogen-like ion.

We begin to describe the case of purely *ionizing plasmas*, i.e. $r_0(p) = 0$, which is sketched in Fig. 3a. In the limit of low electron density, all the excited levels are in the Corona regime, being populated by direct excitation from the ground state and depopulated by spontaneous emission. An increase of n_e results in the descent of the Griem boundary p_G, where levels located over p_G enter in the saturation phase, for which collisional processes prevail over radiative ones. Ionizing plasmas produced in the laboratory (e.g. laser-induced plasmas at early times of plasma formation) are usually *hot* according to the above labeling, so that the low-temperature case is here not described (the reader can find more details in Ref. [4]). It is worth noting that, contrarily to the IB regime, high-excited levels in the saturation region are populated by the multistep ladder-like excitation–ionization mechanism (excitation saturation balance, ESB) and do not reach LTE. In the ESB equilibrium, electrons excited from the ground state into these levels, rather than radiatively decaying again to the ground state, can undergo multi-step excitation and finally result in ionization. For sufficiently high n_e values (i.e. $p_G = 2$), all levels are populated by the ladder-like excitation mechanism.

The improper balances described above strongly reflect on the ASDF and on the fractional ion distribution. In this case, the population ratio n_{Z+1}/n_Z is lower than that predicted by IB (by considering the same values of n_e and T_e); at the same time, the ground state of the energy system is overpopulated with respect to that obtained by IB (i.e. $b(1) > 1$). A sketch of the ASDF of a typical ionizing system is shown in Fig. 4a. Most

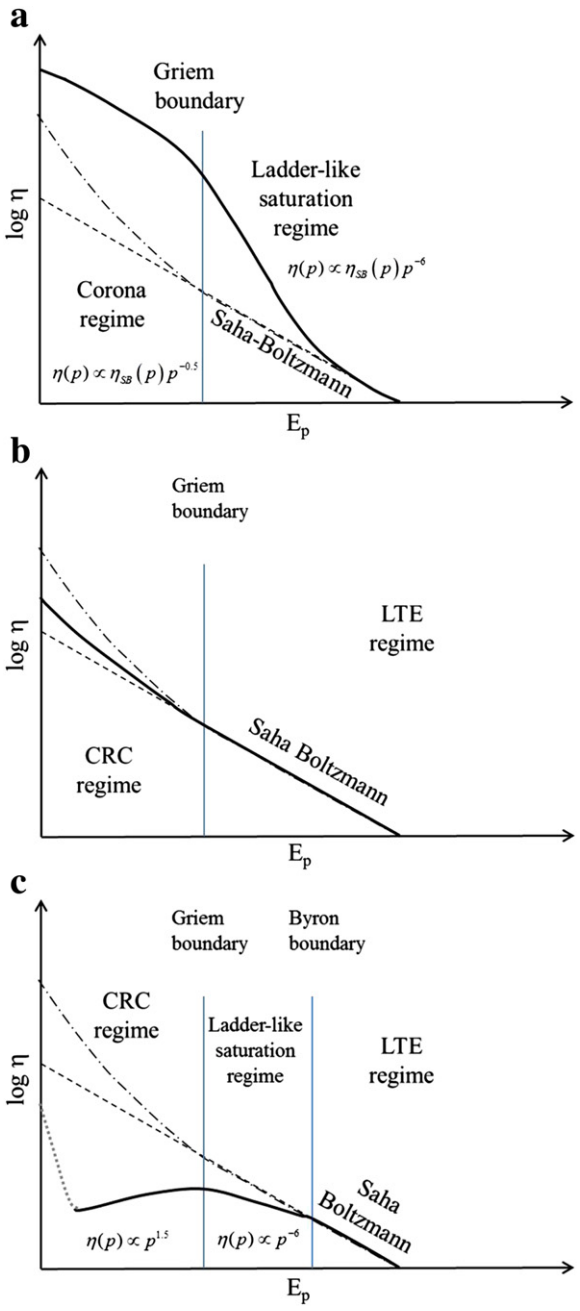

Fig. 4. Boltzmann plot representation of the ASDF, where $\eta(p) = n(p)/g(p)$ and E_p is the energy of the level, for (a) an ionizing system, (b) a hot recombining system and (c) a cold recombining plasma. Dashed and dot-dashed lines represent the population distributions expected for plasmas in LTE and in IB, respectively. In the various regimes, the population dependence expected for hydrogenic systems is reported where $\eta_{SB}(p)$ is the population predicted in LTE. The dotted line in frame (c) is due to the contribution of ionizing component in laboratory plasmas.

of the levels are overpopulated with respect to the ASDF obtained for IB plasmas and thus also with respect to Saha–Boltzmann distribution. It is worth noting that the overpopulation of levels under the Griem's boundary with respect to the IB case – where in both cases population is produced by the ionizing component $r_1(p)$ – is due to the higher population of the ground level in a purely ionizing plasma, i.e. $b(1) > b_{IB}(1)$. The slope of the distribution is therefore not constant and does not allow the calculation of electron temperature. In case of hydrogenic-ions the average population per state in level p, i.e. $\eta(p) = n(p)/g(p)$, where $g(p)$ is the degeneracy of level p, scales as $\eta_{SB}(p) \cdot p^{-0.5}$ in the Corona region, i.e. for lower energy levels,[4] and as $\eta_{SB}(p) \cdot p^{-6}$ in the saturation region, i.e. in the highly excited levels (see Ref. [4] for more details).

The case of purely *recombining plasma*, i.e. $r1(p) = 0$, is sketched in Fig. 3b. In the low electron density limit, all levels are in the capture-radiative cascade (CRC) regime, being populated by radiative recombination and radiative transitions from upper levels and depopulated by radiative decay toward lower levels. With the increase of n_e the Griem boundary p_G climbs down and the levels lying over p_G enter in the saturation regime, i.e. their population becomes driven by collisional excitation/deexcitation processes. Contrarily to the case of ionizing systems, the Byron boundary p_B here plays a fundamental role in the balance reached between levels. Highly excited levels, over the Byron limit, are *hot* ($kT_e \gg \Delta E_{p,p+1}$), while, for sufficiently cold plasmas, it can happen that lower levels are under such limit and therefore they should be considered *cold* ($kT_e \ll \Delta E_{p,p+1}$).

A *hot* level p (i.e. $p > p_B$) in the saturation regime is populated by deexcitation processes from the adjacent upper level $p+1$ and is preferentially depopulated by excitation processes toward the same level $p+1$. This implies that such a level is in thermal equilibrium with level $p+1$ and also with all the upper levels until the continuum states (i.e. with free electrons), since $\Delta E_{p,p+1}$ decreases with p, and then is in partial local thermal equilibrium. This regime can be extended down to all excited levels ($p > 1$) for sufficiently large values of the electron density (i.e. for $p_G < 2$) and of the electron temperature (i.e. for $p_B < 2$). In many cases of recombining cold plasmas, however, some levels are in the conditions for which $p_G < p < p_B$, i.e. they are populated by collisions but they are cold according to Byron's definition. Such levels are populated by collisional deexcitation from upper levels but are depopulated by collisional deexcitation toward lower levels, undergoing a multistep ladder-like deexcitation mechanism (Deexcitation Saturation Balance Equilibrium, DSB). The Byron boundary can thus be considered as a bottleneck of the atomic energy system, since electrons originating from the continuum states and reaching the PLTE states can easily return back to the continuum states, while those crossing downward the Byron limit can no longer cross this boundary and are destined to flow down to the ground state.

The above distinction between hot recombining plasmas and cold recombining plasmas reflects also in the ASDF. In both cases, the population ratio n_{Z+1}/n_Z is higher than that predicted by IB and the ground state of the energy system is underpopulated with respect to that obtained by IB, i.e. $b(1) < b_{IB}(1)$. Moreover, in both cases, the population of highly excited levels is in PLTE. However, in case of *hot* plasmas ($p_B < 2$) the levels following Saha–Boltzmann distribution extend down to the Griem boundary and even the levels below it are very near to PLTE population (for very high temperatures the population of lowest levels can be even higher than Saha–Boltzmann level). Such situation, shown in Fig. 4b, is called pseudo-LTE and depends on the balance between capture and radiative cascade in the high temperature limit [5,24]. Otherwise, in case of cold plasmas (see Fig. 4c), only the highest end of the ASDF, including levels higher than the Byron limit, follows Saha–Boltzmann distribution, while all the lower levels are underpopulated with respect to it. In case of hydrogenic-ions, it is possible to show that the average population per state $\eta(p) = n(p)/g(p)$ scales as $p^{1.5}$ in the CRC region (i.e. for $p < p_G$) and as p^{-6} in the DSB region (i.e. for $p_G < p < p_B$), as discussed in Ref. [4]. It is evident that, also in this case, the experimental slope of the ASDF does not allow the calculation of electron temperature, except by considering only highly excited levels (as for example in [25]).

So far in this section, we have discussed the balances occurring in purely ionizing and purely recombining plasmas, i.e. where $r_0(p)$ or $r_1(p)$, respectively, could be neglected. Although such extreme cases

[4] Actually, the comparison of populations derived by considering $r_1(p) \propto p^{-0.5}$ with CR numerical calculations reveals that the approximation becomes poor at the lowest levels [3].

can be good approximations in some classes of plasmas, in most of the situations both the ionizing and the recombining components should be considered, even where one of them predominates over the other. Generally speaking, the ionization coefficient $r_1(p)$ becomes dominant at low densities and high temperatures, while, on the contrary, the recombination coefficient $r_0(p)$ predominates under the opposite conditions. Moreover, usually the ionization coefficient is considerable for the lowest levels while the recombination coefficient is hardly negligible for highly excited levels. This is the reason why, in laboratory ionizing plasmas, the levels near the continuum are in PLTE (see Fig. 4a), differently from what is expected by the relation $\eta(p) \propto \eta_{SB}(p) \cdot p^{-6}$, and, on the other hand, the population of the lowest energy levels in laboratory recombining systems is much larger than that predicted exclusively by CRC balance (see dotted line in Fig. 4c).

So, to conclude, we can say that the scheme delineated in the present section is significant for understanding the qualitative behavior of ASDF and ion populations in transient and inhomogenous plasmas and their dependence on the plasma parameters. At the same time, it is clear that populations in slightly ionizing and recombining systems should be calculated by accurate CR models which include both $r_0(p)$ or $r_1(p)$ coefficients.

2.5. Criteria for local thermodynamic equilibrium

Among the different balances described in the previous section, special attention must be paid to local thermodynamic equilibrium, because it considerably simplifies the interpretation of spectral line intensities from laboratory plasmas. In this case, the population of all the levels, included the ground level (and therefore the ionization ratios), is driven by collisional processes. Details and criteria concerning Partial LTE can be found in Ref. [26].

According to the description sketched in Section 2.2, in LTE the EEDF has a Maxwellian form defining the temperature T_e of the system, the ASDF is described by the Boltzmann distribution

$$n_z(p) = n_z \frac{g(p)\exp\left(-E_p/kT_e\right)}{U_z(T_e)} \tag{9}$$

and the population of different ionization stages is described by the Saha–Eggert equation

$$\frac{n_e n_{z+1}}{n_z} = 2\frac{U_{z+1}(T_e)}{U_z(T_e)}\left(\frac{m_e kT_e}{2\pi\hbar^2}\right)^{3/2}\exp\left(-\frac{E_{ion}-\Delta E_{ion}}{kT_e}\right) \tag{10}$$

where $U(T_e)$ is the partition function, m_e is the mass of the electron, k is the Boltzmann constant, $\hbar$ is the Planck constant divided by 2π and ΔE_{ion} is the correction of the ionization energy due to the plasma effects. Differently, photons are not coupled with electrons (bound and free) and heavy ions can be not coupled too, so that the kinetic energy distribution of heavy particles (HEDF) and the photon energy distribution cannot be described respectively by Maxwell and Planck distributions at temperature T_e.

The fulfillment of Eqs. (9) and (10) implies $b(p) = 1$ for all levels, which is granted if $b(1) = 1$. In laboratory plasmas such condition is hardly reached because radiative processes cannot be excluded at all and because of the recombination/ionization character of the plasma. Therefore, in practice, the plasma is considered in LTE if $0.1 < b(1) < 10$, i.e. if deviations due to the above phenomena are small.

The previous sections clearly indicate that a plasma is in LTE when a) the population of its atomic energy levels depends only on the collisions (and not on the radiative processes), b) the plasma can be considered quasi-stationary and c) spatial gradients are sufficiently small so that the effects of diffusion can be safely neglected. Such conditions may be expressed by three criteria which should be accomplished to ensure the validity of LTE approximation, i.e. to ensure that $0.1 < b(1) < 10$. In the following we summarize such criteria, derived in Refs. [12,13,15,27,28], which were previously discussed in more detail in Ref. [17].

The condition a) is fulfilled if the electron density is high enough that radiative processes can be neglected for all energy levels or, which is the same, the Griem boundary climbs down to the ground state. The condition is verified when Eqs. (5) and (6), usually known as McWhirter criterion (or sometimes Griem criterion) are fulfilled for all levels. Appropriate corrections should be applied for the opacity effects. Among the conditions a), b) and c), the McWhirter criterion is the most used in the literature and is often considered a sufficient condition to ensure LTE. However, it is necessary to remark that the fulfillment of such criterion is only a necessary condition and does not ensure LTE in case of strongly recombining or ionizing plasmas.

The condition b) accounts for the transient regime of the plasma and is fulfilled if the variation of thermodynamic parameters (T_e, n_e) is small over the times characterizing the establishment of excitation and ionization equilibrium. In that case, the plasma evolves through quasi-steady states and its recombination or ionization character can be neglected. It can be expressed by

$$\tau_{rel} \ll \frac{n_e}{dn_e/dt} \qquad \tau_{rel} \ll \frac{T_e}{dT_e/dt} \tag{11}$$

where τ_{rel} is the time needed by the system for the establishment of excitation and ionization equilibrium. A detailed estimation of τ_{rel} in laser-induced plasmas can be obtained by using a time-dependent collisional–radiative model, coupled with Radiation Transport equations and with a hydrodynamic code accounting for plasma expansion. However, an order of magnitude estimate can be easily obtained by simple considerations. According to the standard CR model, excited levels $n_Z(p)$ reach the equilibrium with the ion population n_{Z+1} much more rapidly than the ground level $n_Z(1)$; therefore the relaxation time is of the order of the time needed to reach the ionization equilibrium, i.e. the equilibrium between $n_Z(1)$ and n_{Z+1}. According to Eqs. (3a) and (3b) and neglecting the spatial relaxation term, the transient phase, during which the population of the two levels relaxes to the equilibrium, lasts for a time approximately given by

$$\tau_{rel} = \frac{1}{n_e(S_{CR} + \alpha_{CR})} \tag{12}$$

where S_{CR} is the total ionization rate and α_{CR} is the total recombination rate, including 3-body, radiative and dielectronic terms. In case of LTE plasmas, however, ionization/recombination occurs mainly via intermediate excited-state levels; therefore, the time needed for the establishment of ionization equilibrium is roughly dictated by the slowest among the collisional excitation processes in the ionization/recombination multi-step chain. Thus, for LTE plasmas τ_{rel} is of the order of the time necessary to reach the equilibrium between ground and first excited levels, as proposed by Griem and Drawin [12,13], i.e. the inverse of the collisional excitation rate between such levels. This can be understood in another way, by considering that near LTE the Griem boundary is lower than the first excited level; therefore, whenever an electron is excited over this boundary, it becomes in equilibrium with the continuum of free electron states and with ions states because of the efficiency of collisional processes. According to Bethe-Born approximation [21] as modified by Van Regemorter [18], for LTE plasmas, τ_{rel} can be expressed by

$$\tau_{rel} \approx \frac{1}{n_e\langle\sigma_{12}v\rangle} = \frac{6.3\cdot 10^4}{n_e f_{12}\langle\bar{g}\rangle}\Delta E_{21}(kT_e)^{1/2}\exp\left(\frac{\Delta E_{21}}{kT_e}\right) \tag{13}$$

where f_{12} is the transition oscillator strength, $\langle\sigma_{12}v\rangle$ is the cross section of inelastic collisions $1 \rightarrow 2$ averaged over the Maxwellian-distributed EEDF, n_e is in cm^{-3} and both ΔE_{21} and kT_e are expressed in eV. The

previous estimate holds for complete ionization of the plasma; in case of partial ionization, the value given by Eq. (13) should be multiplied by the ionization percentage $n_{z+1}/(n_z + n_{z+1})$, which accounts for the fraction of atoms that must be excited. A correction to the value given by Eq. (13) should be applied when self-absorption of the resonance line is present [13]. In cases where the energy gap between ground and first excited level ΔE_{21} is not the largest energy gap in the atomic system, τ_{rel} is the time necessary for establishing the thermal equilibrium between the two adjacent levels separated by the largest gap.

Condition c) accounts for the effects produced by spatial gradients, which are usually caused by the plume expansion and by the dissipation of heat via electron conduction and via radiative processes at the edges of the plume. In case of steep gradients, the diffusion of atoms/ions becomes significant in determining the population of the levels; here (similarly to the case of radiation transport), non-local effects affect the ASDF since the population of excited and ionized states of the atom/ion does not depend on the local values of temperature and electron number density, but rather on the values of such parameters in the region of the plasma from which the atom/ion comes from [12]. It is worth remarking that condition c) accounts for the diffusion-driven deviations from LTE, and not for the spatial variations of concentrations of chemical elements along the plume, which can also occur and are sometimes indicated in literature with the term 'demixing' [29].

The criterion derived from condition c) requires that the diffusion length of atoms/ions, during a time period of the order of the relaxation time τ_{rel}, is shorter than the characteristic length of variation of temperature and electron number density in the plasma [12,27], i.e.

$$\lambda(\tau_{rel}) \ll \frac{n_e}{dn_e/dx} \qquad \lambda(\tau_{rel}) \ll \frac{T_e}{dT_e/dx} \tag{14}$$

where $\lambda = (D \cdot \tau_{rel})^{1/2}$ is the diffusion length during the relaxation time τ_{rel} and D is the diffusion coefficient. The experimental check of such criterion needs an estimate of the diffusion coefficient D of the atoms and of the ions in the plasma, which requires the knowledge of mole fractions and collision integrals of all the species present in the plasma, via a complex multi-component approach. By utilizing the Chapman–Enskog method, which is widely used to calculate the transport properties of gases in the general case, diffusion can be described by calculating $\frac{1}{2}\left(q^2 + q - 2\right)$ ordinary coefficients where q is the number of species present in the plasma [30,31]. A simplified approach was presented by Murphy et al. [32–34], which described the gas diffusion in a binary mixture by introducing four combined diffusion coefficients, accounting for the diffusion due to concentration, temperature, and pressure gradients and to electric fields. Such approach relies however on the assumption of LTE.

In order to simplify the issue, we here consider an approximated approach, where only the species with the largest diffusion coefficient is considered. Usually, the diffusion length of atoms/ions in the ground state is the largest one and therefore the most restrictive, since atoms/ions in the ground state are characterized by the smallest cross section versus collisions. Thus, the relaxation time τ_{rel} to be used for calculating the diffusion length is the same expressed by Eq. (13). In the following, we list some possible situations that can occur in laser-induced plasmas, addressing the reader to more detailed works for a complete treatment of the matter [35].

In case of *cold* plasmas, which are only partially ionized – as for example LIBS plasmas in the cooling stage or inductively coupled plasmas (ICPs) – the diffusion of neutral atoms is the most restrictive for LTE establishment, since atoms have diffusion lengths typically larger than ions. In single-element partially ionized plasmas, the diffusion coefficient of neutral atoms is usually dominated by the cross section of charge–exchange collisions with ions ($A + A^+ \rightarrow A^+ + A$). In fact, among the collisions involving a significant momentum exchange, the charge–exchange cross section is much larger than the cross sections of collisions with other neutral atoms and with electrons.[5] The diffusion coefficient can in this case be expressed (in $cm^2\,s^{-1}$) as

$$D \approx 3 \cdot 10^{19} \frac{kT_H}{n^+ M_A} \tag{15}$$

where T_H is the kinetic temperature of the atoms/ions and kT_H is expressed in eV, n^+ is the absolute number density of ions in cm^{-3} and M_A is the relative mass of the element considered ($M_{Hydrogen} = 1$) [17]. In the case of a cold multi-element plasmas, the diffusion length D of minor and trace elements is generally larger than that given by Eq. (15) since a low amount of ions of the element considered is available for resonance charge-transfer collisions. In this case, the elastic collisions with the background atoms/ions become predominant, which can lead to diffusion lengths of minor/trace element atoms up to one/two orders of magnitude larger than that predicted by Eq. (15) [13]. By considering a binary mixture and by approximating neutral atoms as rigid spheres, the diffusion coefficient (in $cm^2\,s^{-1}$) of the trace species B into the main gas species A can be expressed by

$$D^A_{trace\ B} \approx 1.3 \cdot 10^{21} \frac{(kT_H)^{1/2}}{n_A \sigma^2_{AB} M_{AB}} \tag{15b}$$

where n_A in cm^{-3} is the number density of the main gas, kT_H is expressed in eV, M_{AB} is the reduced mass of species A and B in units of the hydrogen mass and $\sigma_{AB} = (\sigma_A + \sigma_B)/2$, where σ_A and σ_B are effective values of the atomic diameter in Angstrom units [31].

Hot plasmas, where the density of neutral species is negligible, deserve a different approach. The ion collisions with other ions, whose rate is ~$(m_H/m_e)^{1/2}$ times larger than the collisional rate with electrons, are the events limiting the non-local effects in energy state population and the respective diffusion coefficient should be considered here.

The diffusion length of ions is determined by the Coulomb collisions and the diffusion coefficient of the ion species i due to collisions with species i' can be approximately calculated by

$$D_{ii'} \approx 1.29 \frac{(kT_H)^{5/2}}{z^2 z'^2 M_A^{1/2} n_e \ln\Lambda} \tag{16}$$

where z and z' are the charges of species i and i', kT_H is expressed in eV, n_e is in cm^{-3} and $\ln\Lambda$ is the Coulomb logarithm. It is clear that the diffusion lengths of highly charged ions are much lower than those of low charged ones; however, for what concerns the calculation of the diffusion length, this is usually balanced by the larger time τ_{rel} needed by highly charged ions to relax to the thermodynamic equilibrium. In fully-ionized plasmas, other effects strongly affect the ion diffusion as the ambipolar diffusion and the presence of magnetic fields; a detailed discussion about these effects, which are not treated here, can be found in classical plasma textbooks [36,37].

At the end of this section, we want to emphasize that in many laser-induced plasmas the criteria for LTE imposed by the transient and inhomogeneous character are often much more stringent than the criterion needed to ensure the collisionality of the plasma. For this reason, the simplified approach of checking only the fulfillment of the McWhirter criterion can be misleading and should be supplemented by a check of the additional relevant criteria expressed above.

3. Hot plasmas

Here we discuss thermodynamic properties of plasmas produced in vacuum by laser irradiances greater than $10^{12}\,W\,cm^{-2}$. Given the

[5] We note here that in the context of diffusion, the cross section of collisions involving a momentum loss should be considered, e.g. collisions producing large angle scattering. In contrast, when thermalization times among and between plasma species have to be calculated, the cross section of collisions involving energy exchange must be considered.

widespread variety of plasmas included in this class and the complexity of physics to be treated, we here only intend to give a snapshot of the topic, which can be useful to the reader to have a global picture of the situation and to trace similarities and differences with respect to 'cold' plasmas. The interest in such plasmas is usually focused to early times of plasma formation or times immediately successive, that is mainly dictated by their current or potential applications, including the optimization of X-ray, γ-ray and hot particle (electrons, ions) sources, the study of nuclear fusion schemes based on laser plasma compression (i.e. inertial confinement fusion), the investigation of 'warm dense matter' properties which can be useful for astrophysical research, etc. For this reason, attention is also here focused on this time range; longer times of plasma evolution are affected by 'plasma freezing', which is briefly described in Section 4 for 'cold plasmas' induced in vacuum.

3.1. Long and short intense laser pulses

In case of plasmas produced by nanosecond (here: long) and picosecond (here: short) pulses, irradiances greater than 10^{12} W cm^{-2} can be easily achieved with small, table-top lasers. Hot plasmas are often produced by the irradiation of solid targets placed in vacuum as shown in Fig. 5a and exhibit characteristic density, temperature and expansion velocity profiles as shown in Fig. 5b. According to this plot, the electron density can be as high as 10^{23} electrons/cm^3 and temperatures of several keV can be achieved in the underdense plasma region (i.e. in the region where electron density n_e is lower than the critical density n_c, see below) where atoms with atomic number as high as 13 (Al) or 14 (Si) can be almost fully ionized, making H-like and He-like ions the dominant species in the plasma.

While in the very early stage of laser ablation, occurring in the leading edge of the laser pulse, a plasma is formed in front of the target, in a successive stage, covering the most part of the laser pulse duration, the laser light propagates into the plasma only up to the critical density n_c, which is given by $n_c = m_e\omega_L^2/4\pi e^2 = 1.1 \cdot 10^{21}\lambda_L^{-2}$ where n_c is expressed in cm^{-3}, ω_L (sec^{-1}) and λ_L (here expressed in μm) are the laser angular frequency and wavelength, e and m_e are the charge and the mass of the electron, respectively. Electrons oscillate in the laser e.m. field E_L with a quiver velocity $v_q = eE_L/m\omega_L \approx 25\lambda_L\sqrt{I}$ where laser wavelength λ_L and intensity I are expressed in μm and W cm^{-2}, respectively, and the pulse energy is transferred to the plasma mainly via collisional processes (i.e. inverse Bremsstrahlung). As laser light cannot propagate beyond the critical density region, electron conductivity accounts for energy transport beyond this region, leading to the heating of the colder, denser

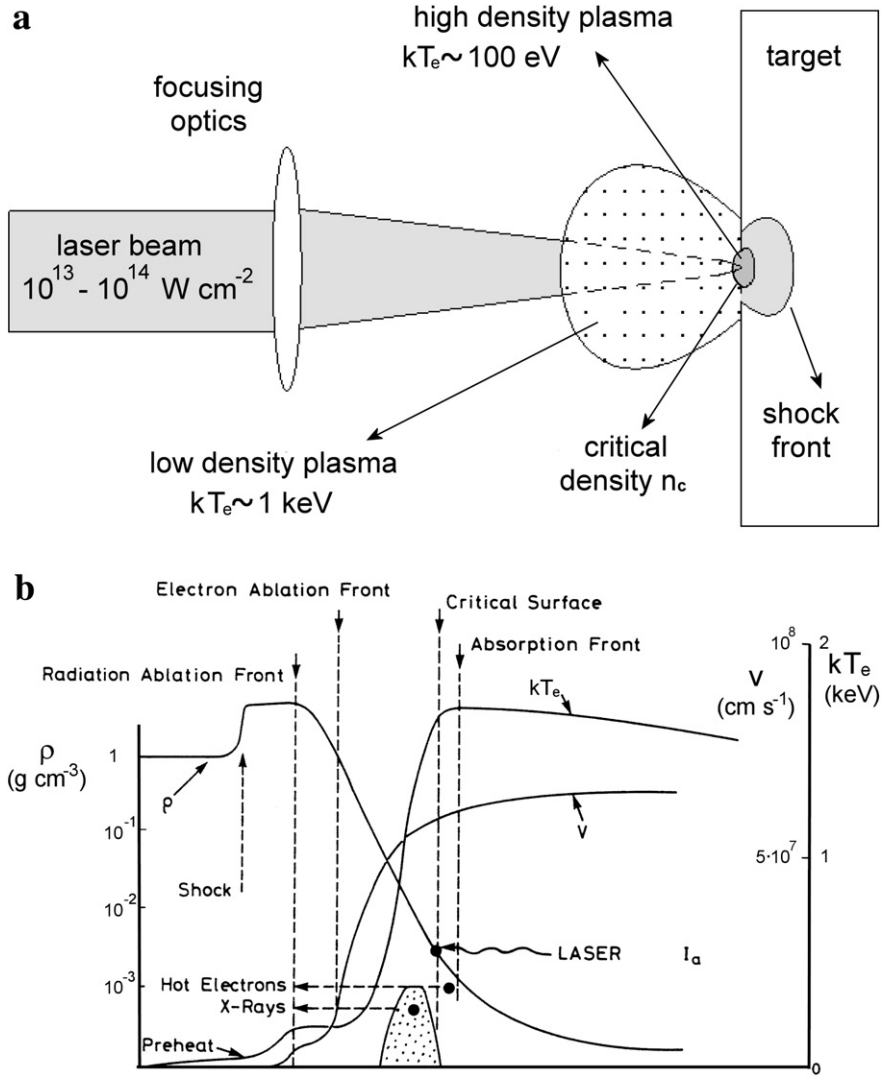

Fig. 5. a) Schematic representation of a laser-induced plasma X-ray source. The laser beam is focused on a massive target and produces a high density plasma from which X-rays and particles are emitted. The low density, hot plasma blow-off which expands in the vacuum towards the laser beam is also shown (not to scale). b) Temperature, density and expansion velocity profiles of a plasma generated by irradiation of a solid target by a nanosecond laser pulse focused at an irradiance of 10^{14} W/cm^2. The figure has been rearranged from Ref. [41].

plasma up to the solid target where ablation and heating of new target material occur.

As the laser intensity increases above 10^{14} W cm^{-2}, the EEDF of heated electrons departs significantly from a Maxwellian distribution, introducing additional complexity in the modeling of spectral emission [38,39]. In fact, at these laser intensities, laser-induced instabilities into the plasma like Stimulated Raman Scattering and Two Plasmon Decay, as well as the onset of resonance absorption mechanism occurring at the plasma critical density, give rise to the formation of longitudinal electron plasma waves. These waves can undergo collisionless Landau damping leading to the production of a component of energetic electrons, which also reflects on the spectrum of X-rays emitted by Bremsstrahlung as shown in Ref. [40]. In these circumstances, the EEDF can be modeled assuming two temperatures, a lower temperature for the "thermal" electrons accounting for most of the electrons and a higher temperature describing the small component of more energetic "hot" electrons.

For relatively long pulses and moderate intensities, for which energy transfer is mainly due to collisional (inverse Bremsstrahlung) absorption, an estimate of the electron temperature of laser produced plasmas in the underdense region, neglecting energy loss mechanisms like radiation emission and plasma expansion, can be obtained by equating the absorbed laser intensity I_{abs} to the electron heat flux. This leads to an electron temperature T_e given by:

$$kT_e = \left(\frac{I_{abs}}{f n_e}\right)^{2/3} m^{1/3} \approx 3 \cdot 10^7 \left(\frac{I_{abs}}{f n_e}\right)^{2/3} \quad (17)$$

where kT_e and I_{abs} are expressed in eV and in W cm^{-2}, respectively, n_e is in cm^{-3} and $f < 1$ is the "flux limiter" parameter that accounts for flux inhibition effects due to deviations from the classical Spitzer description of heat conduction [6]. For typical parameters $I = {}_{abs}10^{13}$ W cm^{-2}, $f =$ 0.1, $n_e = 10^{21}$ cm^{-3}, Eq. (17) gives $kT_e \approx 0.65\,keV$. In the overdense region extending from the critical density layer to the ablation front and whose spatial extent can be of the order of only 10 μm, the electron temperature typically decreases down to less than 100 eV.

In the general case, once the plasma has gained thermal energy, radiation is emitted via free–free, free–bound and bound–bound transitions. Line emission can be profitably used to investigate equilibrium properties of the plasma region from which it comes from. Due to the wide range of electron temperatures in these plasmas, going from tents of keV in the overdense region to a few keV in the underdense region up to tens of keV characterizing 'hot' electrons, different regions of X-ray spectra originate from different regions of the plasma [41]. Typically, the spectral X-ray region below 1 keV derives from the overdense region, that in the range 1–10 keV from the underdense hot region and the most energetic X-rays are produced by free–free Bremsstrahlung radiation from hot electrons. Most of the studies are focused to the emission of the hot underdense region, dominated by bound–bound and free–bound transitions from highly-charged ions. These include the widely studied K-shell spectra and the most-complex spectra originated by L-shells and M-shells, which can be all used to infer temperature and electron density values. In the following, we also will focus on the underdense hot region of the plasma.

In the typical laser-plasma conditions obtained in laboratory, electron density is neither low enough to satisfy the coronal equilibrium (CE) condition, nor high enough for local thermodynamic equilibrium (LTE); then we have the case where both radiative and collisional decay must be taken into account in the collisional–radiative equilibrium, as discussed in Section 2.3. The plasma emission spectrum at a given time during the interaction process can be obtained using an atomic physics simulation code, as for example the kinetic code FLY [42], allowing the rate equations governing plasma ionization to be solved in a collisional–radiative equilibrium appropriate for low-to-medium Z ions (from hydrogen to iron). In the FLY code, the detailed structure of the levels with principal quantum numbers p from 1 to 10 is considered for the H-like ions, while for He- and Li-like simplified hydrogenic formulas are used for $p \geq 6$; only the ground state is considered for lower charge states. The rate equations are solved on a single cell, that is, no spatial dependence is considered. Radiation trapping is included through the so-called escape factors. A more recent version called FLYCHK [43] has recently been developed and provides accurate description of non-LTE equilibrium for low and medium Z plasmas, either in a steady state or in a time-dependent configuration. The modeling of high-Z plasmas requires more complex codes, as for example the HULLAC code [44], able to calculate atomic structure and cross sections for collisional and radiative atomic processes, in the general case.

Such codes use hydrodynamic plasma parameters, including electron density, electron temperature and plasma size, as input parameters. In the case of a time-dependent kinetic modeling, a time evolution of hydrodynamic parameters should be provided as input. Hydrodynamic parameters are usually obtained by means of appropriate hydrodynamic codes simulating plasma expansion (e.g. MEDUSA [45], POLLUX [46], MULTI [47], etc.). In case of quasi steady-state plasmas, the temporal evolution of the X-ray emission is simply obtained by the evolution of the hydrodynamic parameters. In the general situation, however, plasma hydrodynamic conditions may change on a time-scale fast compared to the typical time-scale of atomic processes. In this case, the population of excited and ionized states is not in equilibrium, therefore the steady state approximation is no longer valid, and time-dependent rate equations will have to be solved. In these circumstances, transient processes are set by ionization, excitation and recombination rates [48]. The inclusion of autoionization and dielectronic recombination rates appears crucial, in particular for medium to high Z plasmas, in determining the charge state distribution of low density coronal regions [49].

A quantitative analysis of the transition rates using such modeling tools shows that, in the range of density and temperatures of interest for hot plasmas, excitation and de-excitation processes are in general faster than ionization and recombination processes. Therefore, excited states of a given ion can be considered, in most cases, in equilibrium with the corresponding ground state. Calculations using semi-analytical expressions [50] of the transition rates for aluminum show a dramatic increase of the relaxation time from He-like to H-like ions, compared to ionization from Be-like to Li-like and from Li-like to He-like. This is mainly due to the large increase of the ionization energy of He-like ions involving the tightly bound K-shell electrons. According to these results, the time needed by an aluminum plasma with an electron temperature of 500 eV and an electron density of 10^{21} cm^{-3}, to achieve equilibrium between He-like ions and H-like ions is of the order of several hundred picoseconds. At a density of $1.5 \cdot 10^{22}$ cm^{-3}, relaxation to H-like Al ions is now reduced to a few tens of picoseconds or less, mainly as a consequence of the scaling of the time constant with the electron density. A steady state modeling is therefore expected to provide an accurate description of X-ray radiation emitted during plasma formation by nanosecond laser pulses at a shorter wavelength where the higher value of the critical density, scaling with $\lambda_L{}^{-2}$, leads to energy deposition in the region at higher electron density. In contrast, at longer wavelength laser irradiation, namely lower values of the critical density, more restrictive conditions are established and X-ray emission spectroscopy should be modeled using a time-dependent modeling regime. It should be noted, however, that other processes including, for example, charge–exchange recombination, can contribute to a faster relaxation. In contrast, in the case of lower Z plasmas like oxygen and carbon plasmas, equilibrium is established on a picosecond time-scale or, as in the higher density case, on a sub-picosecond time-scale, making time-dependent calculations not necessary in the case of nanosecond pulses.

From an experimental point of view, the temporal evolution of plasma parameters like electron temperature and density can be inferred by comparison of measured line intensity ratios with the predictions of atomic physics simulation codes based upon collisional–radiative

equilibrium. A common case is the measurement of electron temperature from the intensity ratio between emission lines from different ionization stages. Interestingly, in the case of laser-plasmas, the X-ray source size is very small, typically much less than 1 mm, and extremely bright. In these circumstances, a simple X-ray spectrometer consisting of a flat crystal set in a first order Bragg configuration can be employed to measure emission spectra. Higher spectral resolution analysis can be obtained by using bent focusing crystals, which can also be mounted in configurations allowing a spatial resolution of the X-ray source. The analysis of the temporal evolution of the emission requires the use of fast detectors with sub-nanosecond temporal resolution. X-ray streak-cameras are often used for such purpose. The temporal resolution of such a device can now be as high as a fraction of a picosecond.

As an illustrative example of experimental temperature measurements we consider the case of plasmas generated by irradiation of aluminum targets. In these plasmas, strong line emission from highly stripped Al ions, namely, He-like and H-like ions, occurs, generating the typical resonance series in the range from 1.600 KeV to 2.242 KeV, usually labeled according to the analogous Lyman series of the hydrogen atom. We show the case of time-resolved spectroscopy of a hot, transient plasma produced by nanosecond laser irradiation of an aluminum foil, taken from Ref. [51]. A typical, raw time-resolved X-ray spectrum of K-shell emission, corrected for the geometrical streak-camera distortion, is shown in Fig. 6a. The temporal resolution is about 20 ps. The resonance series of He-like ions and the main resonance line of H-like ions including the corresponding dielectronic satellites [41] are clearly visible. Line ratios obtained from the spectra are compared with simulated ratios calculated with the code suite FLY, applied to hydrodynamic plasma parameters simulated by the hydrodynamic code POLLUX. Match of calculated and experimental line ratios yields a validation of hydrodynamic plasma parameters and of possible deviations from steady-state solutions of energy level population [51,52].

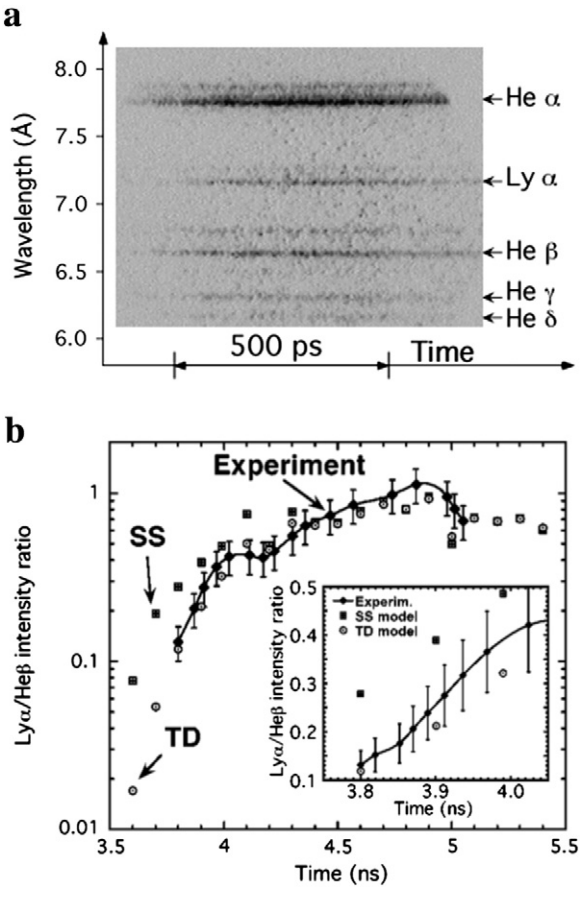

Fig. 6. a) Typical raw time-resolved X-ray spectrum of early K-shell emission from Al plasma observed at 45° from the plasma expansion axis. The resonance series of He-like ions and the main resonance line of hydrogenic ions including the corresponding satellites are clearly visible; b) temporal evolution of the experimental Ly-α to He-β intensity ratio (diamonds + solid line) compared to the intensity ratio calculated assuming a steady-state (square) or a time-dependent (circle) model. The figure has been reproduced with permission from Ref. [51].

In the case of Fig. 6, calculations show a highly localized X-ray emission in a narrow planar slab near the critical density layer, characterized by rapidly changing hydrodynamic conditions, leading to a substantial deviation from the steady-state solution. In Fig. 6b, the experimental ratio of Lyα/Heβ lines, calculated from spectra in Fig. 6a, is reported with steady-state and time-dependent solutions of collisional–radiative rate equations. It is evident that the ion populations calculated by accounting for the transient regime better fit the experimental data for a time lasting a few hundreds of picoseconds. After such time lag, plasma relaxes to a stationary situation, so that steady-state and time-dependent calculations give the same result.

3.2. Ultra-short ultra-intense laser pulses

The scenario described above for long pulses changes dramatically when ultra-short and ultra-intense laser pulses are used, whose duration is much shorter than the typical expansion time of the plasma. The advent of chirped pulse amplification [53] has led to high power lasers capable of delivering several joules in tens of femtoseconds. These lasers allow laser–matter interaction to be studied at irradiances exceeding $10^{20}\,W\,cm^{-2}$. At such high laser intensities the electric field of the laser radiation overcomes by several orders of magnitude the atomic electric field. Matter is ionized in a fraction of the wave period, i.e. almost instantaneously, as can be studied directly by pump and probe interaction in gases [54].

At such very high laser intensities and ultra-short pulses, electrons exhibit relativistic quiver motion and collisional absorption processes (i.e. inverse Bremsstrahlung processes) discussed in the case of long pulses become much less effective. In the case of solid targets, collisionless processes like resonance absorption or the so-called Brunel effect [55] play an important role in the laser absorption in the proximity of the critical electron density n_c. These processes lead to the generation of a significant fraction of hot electrons that in this scenario are referred to as “fast” electrons, even at relatively small laser energies as shown in Ref. [56]. It is worth mentioning that massive production of fast electrons with an ultra-intense laser pulse has been proposed as a possible way to ignite a precompressed target in inertial confinement fusion in the so-called Fast Ignition scheme [57]. In addition to collisionless absorption processes, as in the case of nanosecond pulses discussed above, parametric instabilities like Stimulated Raman Scattering and Two Plasmon Decay also play a role in the laser absorption leading to the generation of plasma waves that contribute to heat the plasma electrons, producing additional fast electrons. In general, experiments show that fast electrons energy can be modeled assuming an exponential distribution. Scaling laws [58,59] have been derived or compared with experiments which can be used to estimate the expected fast electron “temperature” for a given laser intensity on target. These fast electrons give rise, via Bremsstrahlung emission, to hard X-ray radiation, well above the typical thermal emission from such plasmas. According to current ionization models (see for example [60,61]) at the high intensities attainable by ultra-intense femtosecond lasers, the time required to ionize the target is extremely short, so that the plasma becomes opaque to the impinging radiation in a fraction of a period of the laser field oscillation. A strong electron heating is produced in a very short time, so that the electron distribution function is far from a Maxwellian and the plasma, despite the high density, is away from thermal equilibrium. The high density and the high electron kinetic energy make these plasmas bright sources of X-ray bursts, with photon energy extending up to the MeV region. These strong changes in the electron distribution function also reflect in the determination of the

population distribution among levels. Current collisional–radiative models include provision for the component of "fast electrons" as in the code FLYCHK.

A dominant X-ray spectroscopic feature of ultra-short pulse laser interaction with solid targets at high intensity, above 10^{15} W cm^{-2}, is the emission of fluorescence emission from the K-shell of plasma or target ions and atoms due to impact of the fast electrons streaming in the forward direction through the dense plasma towards the solid target. As in any cathode X-ray source, electrons propagate and knock inner-shell electrons out leading to K-shell emission due to transition of electrons into the available K-shell level. Unlike X-ray cathodes, in this laser-driven case, the electron current is so high to be above the Alfven limit [62] and therefore a balancing cold electron return current is generated into the target and allows the fast electron current to propagate. The return current is strongly collisional and gives rise to moderate heating of the target producing a high density relatively low-temperature plasma usually referred to as Warm Dense Matter, which provides a valuable tool for laboratory astrophysics studies [63]. In such plasmas, local thermodynamic conditions may apply with some limitations to the Warm Dense Matter region, but the general description is beyond the capability of analytical or semi-analytical models.

From a theoretical point of view, the complexity of such plasmas makes a fluid description unsatisfactory and the hydrodynamic codes used for plasmas produced by long pulses cannot be used successfully. In the general approach, Particle In Cell simulations are used to where possible. Alternatively, when Particle In Cell simulations are computationally too expensive, hybrid models may be used where the Particle In Cell method is applied for the kinetic description of some species of the plasma, while other species, that can be described by a Maxwell distribution, are treated with a fluid model.

X-ray detection is extensively used in such laser–matter interaction conditions to infer plasma conditions in experiments. A wide class of experiments in this context is indeed carried out using custom made targets with signature layers of known composition. Layered targets are typically used in which the signature layers are buried under the laser interaction layer where the hot plasma is produced. The propagation of fast electron through the signature layers activates characteristic fluorescence emission whose properties carry out information of the local warm and dense plasma conditions. In these circumstances, high resolution X-ray spectroscopy can be used to measure the exact structure of K-alpha emission, including width and shift, to determine temperature and density of the emitting dense plasma (Ref. [64] and references therein). At the same time, high-resolution X-ray imaging provides key information on the divergence of the fast electron beam, a crucial parameter that controls the energy deposition inside the material.

4. LIBS plasmas

In this section the attention is focused on the occurrence of local thermodynamic equilibrium in LIBS plasmas. These are usually induced by laser pulses in the irradiance range 10^{8}–10^{12} W cm^{-2} and are typically colder and less dense than those described in the previous section. In the typical temporal window of observation, usually extending from a few hundred nanoseconds to several microseconds or tens of microseconds after the end of the laser pulse, the electron temperature kT_e is in the range 0.5–3 eV and the electron density n_e in the range 10^{16}–10^{19} cm^{-3}. These characteristics place the LIBS plasmas in the wider class of thermal or pseudothermal plasmas, which are approximately in the LTE state at least in some temporal windows or spatial regions, and include among the others the ICP plasmas and the DC or RF discharge plasmas.

The interest in the subject is motivated by the need of establishing the optimal experimental conditions for obtaining reliable quantitative analysis of materials via the LIBS technique. In particular, substantial deviations from LTE can strongly invalidate the quantitative results obtained by Calibration-Free methodologies (CF-LIBS, see Ref. [65] and references therein), which calculate the concentration of the different plasma species by assuming that the population of the atomic/ionic levels is described by the Saha–Boltzmann distribution.

The present chapter is mainly focused on plasmas induced in air at atmospheric pressure and in particular on their cooling stage, occurring after the laser switched off, which is the most common condition for LIBS measurements. In the paragraph devoted to the ionization–recombination balance, however, the plasma thermodynamic states during the laser ablation process and in case of expansion in vacuum or in a low-pressure environment are also briefly discussed.

Three possible approaches can be utilized to investigate the occurrence of LTE in LIBS plasmas. The first approach relies on the direct measurements of the level population into the plasma, or, which is similar, on the measurements of the temperatures characterizing the ASDF or the charge state distribution (or portions of these distributions) and the temperature describing the kinetic energy of electrons and heavy particles.[6] The temperatures obtained are compared successively for consistency. This approach is used in a considerable number of works, as for example in Refs. [66–74]. The second approach, which is indirect, consists of checking the LTE criteria described in Section 2.5, i.e. the McWhirter criterion and those concerning the transient and the inhomogeneity nature of the plasma. Very few papers check the fulfillment of all the criteria [25,75,76], while most of them take into account only the McWhirter criterion, which constitutes a necessary but not a sufficient condition for LTE. Finally, the issue of LTE in LIBS plasmas can be investigated by theoretical modeling (Ref. [77] and reference therein), using CR or analytical codes. Few authors utilized this approach [10,78–80] and only very few papers make use of time-dependent modeling [10,78,81], which is fundamental to establish the relevance of recombination and ionization in determining level population. To our knowledge, none of the theoretical works published so far tackled the issue of non-LTE effects produced by atom/ion diffusion.

Outlining the framework concerning the thermodynamic state of LIBS plasmas is not an easy task. The literature dedicated to the issue is limited and the results obtained are often partial, not comparable and sometimes even contradictory. After describing the main experimental techniques that can be used to measure the different plasma temperatures in Section 4.1, the problem of LTE is discussed by tackling separately the issues expressed by the LTE criteria, i.e. the balance of radiative–collisional processes, the balance of ionization–recombination due to the rapidly varying plasma parameters and the possible deviations produced by plasma inhomogeneity.

4.1. Plasma temperatures and diagnostics

When Complete Thermal Equilibrium holds, the population among atomic (and ionic) excited levels, ionization stages, translational states of electrons and heavy particles, as well as photon energy states can be described by the well-known Boltzmann distribution, Saha–Eggert equations, Maxwell and Planck distributions, respectively, all taken at the same temperature value, i.e. $T_{exc} = T_{ion} = T_e = T_H = T_{ph}$. However, when deviations from CTE are present – i.e. some improper balance occurs between the energy levels – departures from the above statistical laws are produced or, which is the same, the temperatures *measured* from the various distributions can differ from each other.[7]

Because of the escape of radiation from the plasma the distribution of photon energies is always decoupled from those of electrons (free and bound) and heavy particles in the plasma, so that the measured *photon temperature* T_{ph} is different and usually lower than the other

[6] We here recall that the kinetic energies are distributed among a continuum of energy states.

[7] One should note here that in non-LTE plasmas the populations of the energy levels can no longer be described by the abovementioned statistical laws, so that the measured value of the temperature refers to a few levels or corresponds to an average over the levels.

temperatures. As an example, David et al. [82], focusing a 65 ns ruby laser pulse on a carbon target at ~10^9 W cm^{-2} in vacuum, measured a photon temperature of 0.7 eV (at the end of the laser pulse), which was lower than the excitation (~1 eV) and the electron temperatures (~8.5 eV). Similarly, De Giacomo et al. [83], focusing a 8 ns Nd:YAG laser pulse ($\lambda = 532$ nm) on a Ti target in air at ~$3 \cdot 10^9$ W cm^{-2}, measured the photon and excitation ionic temperatures in the temporal range 0.25–3 μs, finding a significant discrepancy which reduced with the delay time.

The temperatures characterizing the translational motion of the electrons and of the heavy particles (i.e. describing the EEDF and the HEDF) are named the *electron and heavy particle temperatures* T_e and T_H, respectively. In some papers the temperature of heavy particles is also named the gas temperature. T_e is usually calculated by measuring the continuum contribution in the emission spectrum (via the line-to-continuum ratio or via the absolute continuum emission methods) [66,84–86] or through the Thomson scattering by using an external light source [87]. The simultaneous measurement of Thomson and Rayleigh scattering can provide both the values of electron and gas temperatures [88,89]. In many papers, the heavy particle temperature T_H is also estimated by measuring the rotational T_r or vibrational T_v temperatures of molecules present in the plasma [90–93], by assuming that $T_H = T_r = T_v$; this approach is justified by the strong effectiveness of energy exchange between translational and roto-vibrational states of heavy particles. Other techniques that can be used to estimate plasma temperatures can be found in Ref. [94] and in the references therein. As reported in the theoretical section, due to the large Coulombian cross section between charged particles, in typical LIBS conditions the bulk of electrons and heavy particles can be described by Maxwell distributions, where deviations are possible in the high energy tail of the distribution [8]; significant deviations to this picture can be present only for ionization degrees as low as 10^{-4} [9]. However, due to the inefficiency of kinetic energy transfer between electrons and heavy particles, the transient character of laser-induced plasmas can lead to a decoupling of their temperature, i.e. to a 2-T plasma state [5], in particular situations, as discussed in Sec. 4.3. Apart from cases of very low plasma ionization, however, electron collisions are much more effective than ion collisions in inducing the excitation of a bound electron, so that the temperature of Saha–Boltzmann distribution, describing the ASDF of atoms/ions at thermal equilibrium, is the temperature of the electrons T_e [5]. Therefore, although a 2-T plasma of the kind above-described cannot be fully considered as an LTE state, it usually does not produce significant deviations in plasma spectroscopy.

The temperature characterizing the atomic state distribution function is usually called the *excitation temperature* T_{exc}. In case of non-LTE plasmas, the measured T_{exc} is not the same in different portions of the ASDF and approaches the value of the electron temperature T_e for highly excited states [95]. T_{exc} is usually measured through the Boltzmann or Saha–Boltzmann plot of the emission lines, where the second approach makes use of lines deriving from different ionization stages and thus assumes the ionization–recombination equilibrium. One should note here that both the approaches have the limitation of being unable to probe the population of the ground level. This point is extremely important and casts doubt on the use of this method to assess LTE in a plasma. In fact, the ground level is the state more prone to non-LTE deviations induced by the radiative decay and has the longest relaxation time to equilibrium and the largest diffusion length. We want here to point out two different methodologies that can be used to tackle this problem. The first method is the construction of a Boltzmann plot by using *absolute* line intensities. Such technique, which can be indeed challenging from an experimental point of view, has the advantage that also the ground state population can be plotted, after it has been calculated by using the ideal gas law with the experimental gas temperature [95]. The second method is the construction of a special Boltzmann plot by utilizing self-absorbed lines, where the population of the energy levels, including the ground, can be calculated from the quantification of self-absorption of optical transitions [96] and, consequently, of the optical depth of the lines. Such method allows the calculation of the excitation temperature of the lower energy part of the ASDF that can be successively compared to that of the highly excited levels, calculated through the traditional Boltzmann plot technique [96]. Other ways to measure the excitation temperature, which however have been rarely used in LIBS plasmas, are those making use of laser-induced absorption or fluorescence, where the former allows also the quantification of the ground state population (see Ref. [96] for references).

Another way to assess the departure from LTE condition due to lack of ionization/recombination balance is that of comparing the population ratio of two energy levels belonging to a neutral atom and to a positive ion, as calculated by measured line intensities, with the ratio predicted by the Saha–Eggert equation at the measured electronic or excitation temperature. Alternatively, in some papers, the above ratio is used to calculate the temperature value that is predicted by the Saha–Eggert equation and such value is named *ionization temperature* T_{ion}. We want here to remark that T_{ion} does not have a real physical meaning, when ionization–recombination equilibrium is violated.[8] However, this approach is immediate and useful to assess departures from such equilibrium, so that it has been utilized in many LIBS works [67–71,74]. It is worth to remark that the results of this method can be strongly affected by the presence of temperature spatial gradients in the plasma, which produce a different spatial distribution of neutral and ionized species. The non-uniformity of electron temperature produces also a distinction of excitation temperatures measured from neutral and singly ionized species or even from neutral atoms originating from elements with different ionization energies, due to the different spatial distributions of the emitters, as shown in some papers [97,98]. Therefore, as suggested by Aguilera et al. [97], spatially-resolved measurements are needed to fix these problems.

4.2. Collisional vs. radiative processes: the McWhirter criterion

All the papers dealing with LTE in LIBS plasmas make use of the McWhirter criterion, reported in Eq. (6), which expresses the conditions for which the collisional processes prevail upon the radiative ones in populating the excited levels. This occurs whenever the plasma electron density is larger than a certain threshold slightly depending on the electron temperature. Most of the papers, however, refers to such a criterion as it were a sufficient condition for LTE, while it is actually only necessary but not sufficient, and therefore assumes the presence of LTE whenever Eq. (6) is fulfilled.

In a previous paper [17], several considerations on the McWhirter criterion in LIBS plasmas were already reported; there, in particular, the effects of plasma composition, background gas pressure, self-absorption and delay time of acquisition were discussed. Here, we give a brief summary of these points, making use of some experimental results reported in the literature.

In Fig. 7 the trends of the measured electron density and of the electron density needed for the fulfillment of the McWhirter criterion for various plasma species, calculated by utilizing the experimental values of the electron temperature, are compared. The data plotted in the figure were obtained by rearranging the results of Barthelemy et al. [68] (Fig. 7a), and of El Rabii et al. [99] (Fig. 7b). In Ref. [68] the plasma was obtained by focusing a XeCl laser pulse ($\lambda = 308$ nm, $\tau = 10$ ns) onto an aluminum target (with traces of Fe and Mg) in air. The work in Ref. [99] investigated the plume induced by focusing a Nd:YAG laser pulse directly in air at atmospheric pressure ($\lambda = 355$ nm, $\tau = 7$ ns). These results, for consistency, will be also used in the following

[8] The Saha eq. is obtained by considering the thermodynamic equilibrium between excited levels and free electron states; therefore, its temperature dependence derives from two terms, accounting for the electron temperature and the excitation temperature in the ASDF.

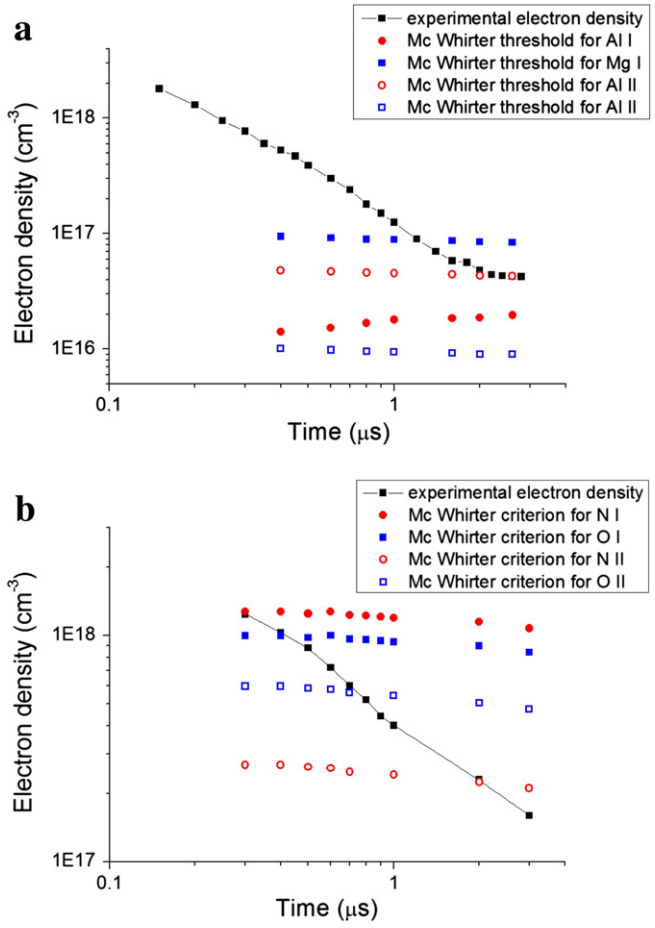

Fig. 7. Fulfillment of the McWhirter criterion, expressed by Eqs. (5) and (6), for several plasma species at different evolution times. The McWhirter thresholds have been calculated by utilizing the experimental values of the electron temperatures.
The data were rearranged from the works of Barthelemy et al. [68] (a) and El Rabii et al. [99] (b).

paragraphs to discuss the effects of the transient and inhomogeneity nature of the plasma.

Fig. 7 shows that the criterion is generally fulfilled at early times because of the high value of the electron density, which makes the collisional excitation/deexcitation and ionization/3-body recombination processes very effective. At a certain time, depending on the species, the radiative processes tend to become predominant and LTE is violated. The time when it occurs depends on the extent of the largest energy gap between adjacent levels in the atomic system, which usually coincides with the gap between the ground and resonant excited levels, as tabulated in Table 1 of Ref. [17]. Non-metal species usually have larger energy gaps and therefore require much larger values of the electron density for the fulfillment of the criterion; therefore, for non-metal species, the criterion is fulfilled only at early times ($t < 300–400$ ns in Fig. 7b). Metal species, on the other hand, usually fulfill the criterion for longer times, which often overlaps with the time of LIBS signal acquisition. It is also worth remembering that the self-absorption of the resonance line, which is often strong at late times for neutral species, leads in a lowering of the threshold by roughly an order of magnitude, which contributes to the fulfillment of the criterion, especially for metal species: in Fig. 7a, for example, self-absorption of the resonance line of Mg I at 285.2 nm, here non-quantified, could result in the fulfillment of the criterion even at times larger than ~1 μs.

Travaillè et al. [80] developed a CR model, based on a set of atomic data obtained by an optimized effective potential method, for investigating the deviations from LTE in a steady-state and homogeneous plasma. Considering the case of aluminum, they showed that the McWhirter criterion well agrees with the threshold given by the CR model, and that in typical LIBS conditions, the aluminum plasma is in LTE, which agrees with Fig. 7a. They also showed that the ionic species are more restrictive than the neutral ones by one order of magnitude on n_e, because of the largest energy gap between ground and first excited levels. However, by considering the McWhirter criterion expressed by Eq. (6), which accounts for quantum-mechanical corrections via the thermally averaged effective Gaunt factor $\langle \bar{g} \rangle$, one may find that, under low-temperature conditions, the criterion is more restrictive for neutral species (e.g. Mg species in Fig. 7a and N and O species in Fig. 5b), since their $\langle \bar{g} \rangle$ factor is lower by a factor ~10, as pointed out in Sec. 2.3 [18–20].

When laser ablation occurs in vacuum or at reduced background pressure, the stage at which the radiative processes prevail upon the collisional ones shifts to much earlier delay times because of the fastest expansion of the plume.

It is also worth noting that the criterion can be fulfilled in the inner region of the plume but not in its periphery, as shown in Ref. [17], where the spatial- and temporal-resolved measurements of Aguilera et al. [100] (Fe target, $\lambda = 1064$ nm, $\tau = 4.5$ ns) were utilized for the purpose. It was there shown that, at 1000 mbar, the criterion is fulfilled in the 0.5–1 μs temporal range in all the measured plasma regions, while at later times it is verified only in the core of the plasma and not in its periphery. Differently, in the case of plasmas induced at 10 mbar, the criterion is fulfilled only in the 0.5–1 μs time window, while it is not verified at later times. A similar conclusion was drawn in Ref. [101], where the Calibration-Free approach for quantitative analysis was tested on radially resolved spectra from a copper-based alloy. It was there shown that the concentration of elements in the core of the plasma was very close to the nominal composition, while a discrepancy was found by using the spectra emitted from the outer regions. This was explained by the gradual departure of the plasma from local thermodynamic equilibrium conditions at increasing plasma radius values, due to the significant decrease of the electron density in the external shells of the plasma.

4.3. Dynamic evolution of the plasma: ionization vs. recombination

Even in the cases where collisional processes prevail against radiative ones, which are often verified in LIBS plasmas, the transient nature of the plasma can put severe constraints for the fulfillment of the LTE condition. When the evolution is too rapid, in fact, the plasma does not have enough time to reach the ionization equilibrium and can be significantly ionizing or recombining. Rearranging the first condition of Eq. (11), which is the most stringent in an expanding plume, by using Eqs. (3b) and (13), this occurs when

$$\frac{1}{n_e}\frac{dn_e}{dt} = \frac{1}{n_e}\left[\left(\frac{dn_e}{dt}\right)_{\text{exp}} + n_e n(1) S_{CR} - n_e n^+ \alpha_{CR}\right] > n_e \langle \sigma_{12} v \rangle \qquad (18)$$

where the left hand side (l.h.s.) represents the rate of electron density variation and the r.h.s. is the rate of collisional excitation to the first excited energy level (or to the upper level of the largest energy gap). In the equation n_Z and n_{Z+1} were substituted by n and n^+, indicating the density of neutral atoms and singly-charged ions, because in LIBS plasmas these are the two most populated charge stages.[9]

The former rate depends on two terms, accounting respectively for the electron depletion due to plasma expansion $(dn_e/dt)_{exp}$, deriving from the spatial relaxation term $\nabla \cdot n_e w$ in Eq. (3b), and for the combined effect of total ionization and recombination processes $n_e n(1) S_{CR} - n_e n^+ \alpha_{CR}$. As we shall see in the following paragraphs, the expanding nature of the

[9] During the laser ablation process, especially for metal species, the density of doubly-ionized species can be no more negligible, and ionization/recombination equilibrium between singly- and doubly-ionized species should be considered.

plasma, via the term $(dn_e/dt)_{exp}$, strongly affects the characteristic times of plasma evolution and therefore the attainment of LTE.

4.3.1. Early phase of laser heating

The LIBS user is mainly interested in the state of the plasma during the cooling phase; nevertheless, it is useful to sketch rapidly what happens during the *plasma formation*, both for the sake of completeness and because the early phase constitutes the starting point and thus the boundary condition for the following evolution stages. When the laser pulse is on, the photon energy is absorbed via inverse Bremsstrahlung or photoionization processes and then converted into thermal energy of the electrons that rapidly thermalize and reach a Maxwellian distribution. By considering typical values of electron density and temperature during the LIBS plasma formation, it can be shown that electron–electron relaxation time τ_{rel}^{ee}, as given by Eq. (1), is of the order of tens or hundreds of femtoseconds, that is, in most of the cases, much shorter than the pulse duration. This also implies that when a fs laser pulse is used, significant deviations from Maxwell distribution can be expected in the EEDF at the end of the laser pulse.

Due to the inefficiency of energy exchange between electrons and heavy particles, during the laser absorption the gas can remain colder, as shown for example in Amoruso et al. [102]. Such 2T-condition depends on the larger thermalization time τ_{rel}^{eH} between electrons and ions, which, according to Spitzer formulation, is $\sim \frac{m_H}{m_e}\tau_{rel}^{ee}$. In typical LIBS conditions τ_{rel}^{eH} is of the order of the nanosecond, which can be longer than the plasma heating time, in particular in case of ps- and fs-laser ablation. Relying on the above scaling of the relaxation times, the 2T-condition should rapidly cease at the end of the laser pulse [102,103], although some experimental measurements suggest that different T_e and T_H can persist for a much longer time [72,89,91].

Much more important for the plasma diagnostics are the deviations from LTE in the population of the levels and of the ionization stages. These often occur since the scaling time of plasma heating, which is of the order of the laser pulse duration, is in many cases shorter than the relaxation time given by Eqs. (12) and (13). The relaxation time for metal species is typically of the order of the nanosecond while that for air species and typical background gas species (Ar, He, etc.) is larger by 2–3 orders of magnitude. This implies that deviations from LTE are expected to be much more severe in case of short and ultra-short pulses. Moreover, significant deviations are also expected in case of breakdown occurring directly in gas, because of the long relaxation time of gas species as N, O, Ar, He, etc.

During the laser heating, the rate of electron density variation in Eq. (18) is dominated by the ionization term, which is much larger than the expansion and the recombination terms. The ASDF and the charge state distribution are therefore those typical of an ionizing plasma (see Fig. 4a). It is worth noting that in case of ns laser pulse, the presence of a background gas can result in the onset of a Laser Supported Detonation regime, which significantly modifies both the scaling time of plasma formation [104] (i.e. the expansion term in Eq. (18)) and the relaxation times of plasma species (because of the change of n_e and T_e), so that the issue should be checked case by case.

A confirmation of this scenario can be found for example in David et al. [82] and in Ogino et al. [105,106]. David et al. [82] irradiated a graphite slab in vacuum by using a Q-switched ruby laser ($\tau \approx 60$–70 ns, $I = 10^9$–10^{10} W cm^{-2}) and measured, via interferometric and spectroscopic techniques, the temperature of the electrons T_e and that given by Saha equation T_{ion} at the end of the laser pulse. The results showed that the electron temperature is larger than the Saha temperature by a factor of ~8 at the laser irradiance $I = 10^9$ W cm^{-2}, and that this discrepancy reduces at larger laser irradiance values, reaching a LTE condition already at the end of the pulse at $I = 10^{10}$ W cm^{-2}. The condition $T_{ion} < T_e$ is typical of an ionizing plasma, since the low value of T_{ion} denotes an overpopulation of neutral atoms with respect to ions. The condition $T_{ion} \approx T_e$ obtained at larger irradiance is explained by the authors by the steeper growth of electron density and energy in the leading edge of the laser pulse, leading to a higher ionization rate; this results in a higher value of T_{ion} and correspondingly in a lower value of T_e – part of the thermal energy of the electrons is spent for the ionization – at the end of the laser pulse, as experimentally measured.

Ogino et al. used a time-dependent CR model to simulate the early phase of plasma formation in Ar [105] and in air [106], showing that the ionizing character of the plasma induces a faster propagation of the blast wave in the medium, as experimentally found, and a transient non-LTE excited state distribution.

4.3.2. The plasma cooling stage

When the laser pulse switches off, the plasma continues to expand and cool, both as a result of energy conversion from thermal to translational and of the interaction with cold molecules of the background gas. The plasma is therefore recombining. However, depending on the fulfillment of Eq. (11), the plasma can still be in LTE. It is evident that the nature and the pressure of the background gas strongly affects both terms of Eqs. (11) and (18), i.e. the timescale of plasma decay and the relaxation time toward thermal equilibrium. Here, in order to give a picture of the phenomenon we consider the cases of plume expansion in vacuum and in background gas at atmospheric pressure, being the latter the most common LIBS condition. Other experimental conditions which apply to particular LIBS applications, as for example measurements at reduced or high pressures (e.g. for space exploration, analysis inside furnaces or underwater, or in combustion engines environments), should be investigated case by case.

Regarding the case of expansion in *vacuum*, let's consider for a while the adiabatic spherical expansion of a fully ionized gas. This scheme is not applicable at early times when the expansion is planar (it also neglects the occurrence of ion recombination). In this model, the conservation of mass requires that the velocity of a fluid element is proportional to the radius and does not depend on the time, i.e. $r \propto t$, which implies that the electron density falls as $n_e \propto r^{-3} \propto t^{-3}$. The adiabatic expansion, at the same time, implies that the temperature decreases as $T_e \propto t^{-3(\gamma-1)}$, and thus for $\gamma = 5/3$, $T_e \propto t^{-2}$. If we assume that the plasma is in LTE at the end of the laser pulse and we consider Saha equation, it is evident that the scaling laws described above lead the system out of LTE during the following evolution, since the r.h.s. in Eq. (10) falls more rapidly than the l.h.s. term because of the presence of the exponential term; physically, this depends on the fact that the ionization rate falls very rapidly when the temperature becomes lower than the ionization energy. Such imbalance of ionization equilibrium, occurring approximately when $kT_e \approx E_{ion}$, implies that the effect of ion recombination should be considered to describe the plasma evolution. Rumsby et al. discussed such an issue, showing that the recombination does not produce significant variations in the electron density decay rate except at late times of expansion, and therefore the behavior continues to be valid even if recombination is taken into account, as experimentally confirmed [107]. This means that the sum of the second and third terms on the l.h.s. of Eq. (18) is negligible. Conversely, the effect of recombination on the plasma temperature is significant, since recombination releases thermal energy to free electrons and significantly changes the rate of temperature decay. Both by modeling and by experimental approach, it has been shown that for sufficiently ionized plasmas, recombination reduces the cooling rate of the plasma, which asymptotically acquires the dependence $T_e \propto t^{-1}$ [108]. The transfer of energy to free electrons, in turn, can stop the ion recombination so that the degree of ionization becomes frozen at a certain time, as experimentally observed [78,109,110]. The scaling law $T_e \propto t^{-1}$ also implies an increase of the electron–ion collisional times ($\tau_{rel}^{eH} \propto t^{1.5}$), which produces a decoupling of electron and ion temperatures at late times of the expansion [107].

Deviations from LTE can be present much earlier than the 'freezing time', which can be of the order of a few microseconds. Just to have an idea, the expansion timescale of the plasma and the relaxation times of singly-ionized carbon species, calculated and extrapolated from the

data published by Rumsby et al. [107] ($\tau = 20$ ns, $I = 7 \cdot 10^{10}$ W cm^{-2}, carbon target) are plotted in Fig. 8. It is evident by the figure that both the expansion timescale and even more the relaxation time of plasma species noticeably change during plasma evolution. The relaxation time of singly-ionized carbon is much lower than the expansion timescale for times lower than ~200 ns, suggesting that LTE can be present in this range, while it becomes much higher at late times of evolution.

Now, we discuss the case of LIBS measurements performed *in air at atmospheric pressure* by using the same approach used for the vacuum case, since recombination–ionization processes and plume expansion are strictly related. Such an approach, even if not decisive in practical cases for determining the violation of LTE, can be useful for sketching the occurring phenomena and is quite new in the LIBS forum.

When laser ablation is carried out in air, in the cooling stage the expansion of the plume is much slower than that occurring in vacuum, which strongly affects both the rates of cooling and of electron depletion. The expansion of the plasma plume in the background gas can be described by the point strong explosion model solved by Sedov [111], as experimentally verified in many investigations [112–115]. The self-similar solution formulated by Sedov predicts that the blast wave expands in spherical geometry as $r_{SW} \propto t^{2/5}$ at early times of plasma evolution (lasting for a few microseconds), while corrections should be applied at later times when the counterpressure of the background gas becomes comparable to the pressure behind the shock wave (SW). At the end of the laser pulse, the plasma is in contact with the SW, which is able to ionize the background gas [114]. However, since the plasma cools during the expansion and the SW rapidly weakens, the plasma detaches from the SW front at times of the order of hundreds of nanoseconds and stops at a radius of the order of a mm [113]. Therefore, the expansion of the plasma can be roughly subdivided into two phases, a first one following blast point wave model and a second one dominated by the background gas confinement.

In the former phase, the rate of electron depletion in Eq. (18) is usually dominated by the expansion term $(dn_e/dt)_{exp}$, similarly to the vacuum case. According to the strong point explosion and considering a spherical symmetry, the particles density (and then also the electron density) near the center of the explosion goes as $n_e \propto t^{-6/5\gamma}$, which becomes $n_e \propto t^{-0.86}$ for $\gamma = 7/5$ [116]. Similarly, for planar expansion, which can be applicable for large focal spots and early times of expansion, electron density goes as $n_e \propto t^{-0.48}$. Such trends account only for the effects produced by the plume expansion and neglect both recombination and diffusion processes. Here, differently from the vacuum case, where the expansion is much more rapid, the occurrence of recombination–ionization processes brings a significant contribution to the rate of electron depletion, i.e. the sum of 2nd and 3rd terms in Eq. (18) is not negligible with respect to the 1st term. More precisely, this contribution is negligible at early times but becomes more and more important with increasing the delay from the laser pulse, resulting in a more steep decrease of electron density, going as $n_e \propto t^c$ with $c < -0.86$. This can be clearly seen in Fig. 9, obtained by rearranging the data obtained by Barthelemy et al. [68], which shows the trend of electron density and the instantaneous value of the coefficient c as a function of time. Fig. 9 shows that at early times ($t < 150$ ns) the c value changes from ~ −0.5 to ~ −0.8, denoting the transition from planar to spherical symmetry expansion, and that it progressively decreases with time, due to the increasing contribution of recombination processes [116], up to 1 μs. The change of the trend at ~1 μs is due to the fact that background gas counterpressure is no more negligible and the plume progressively slows down and finally stops, so that the expansion term in Eq. (18) becomes negligible with respect to the other two terms in the l.h.s. The residual depletion of electrons at times larger than ~1 μs is produced by the recombination. The change of regime in the plume expansion was observed in other experiments to occur in the delay time range 300 ns < t < 1500 ns [117,118].

Values of c coefficients lower than −0.86, and therefore denoting the presence of ion recombination, can be easily obtained also by rearranging other data published in literature regarding LIPs produced in air [70,97,116]. Similarly, Dzierzega et al. [89], focusing a Nd:YAG laser pulse ($\tau = 4.5$ ns, $\lambda = 532$ nm) in He at atmospheric pressure at ~$2.5 \cdot 10^{11}$ W cm^{-2}, found a coefficient $c = -0.9$, lower than the value $c = -0.72$ predicted by the point strong explosion theory in spherical symmetry in a monoatomic gas ($\gamma = 5/3$). Litvak et al. [116] investigated laser produced plasmas in hydrogen gas at 1–70 atm, showing that the contribution to electron depletion due to ion recombination increases with time both in the blast wave expansion phase and in the quasi isothermal phase, confirming the framework delineated above. As in the vacuum case, it can be also shown that the presence of recombination leads to a smoother decrease of plasma temperature, if compared to the adiabatic trend, due the release of thermal energy to free electrons by the recombination process.

In the temporal range $t > 1$ μs, electron depletion is mainly due to recombination processes. The expansion is inhibited, because of gas confinement. In this phase the plasma loses thermal energy by diffusion and by collisions with cold background atoms, which is however partly balanced by the release of energy produced by electron–ion recombination rapidly converted into thermal energy. This balance results in a smooth decrease of electron density and temperature, so that, often, this temporal range is referred as quasi isothermal phase. The slow cooling rate due to the confinement effect, on one side, results in an increase of the characteristic time of plasma expansion and then favors the attainment of thermal equilibrium. On the other hand, however, the plasma in this phase can be significantly recombinant because the

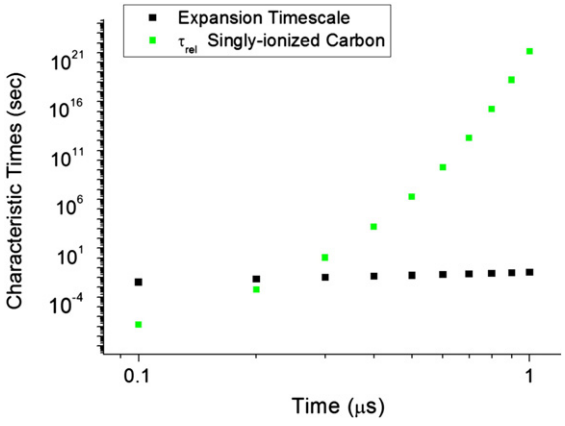

Fig. 8. Timescales of plume expansion and relaxation times of singly-ionized carbon species, calculated from data in Ref. [107], where the ionization degree is $Z = 1.8$, slightly changing in the observed temporal window.

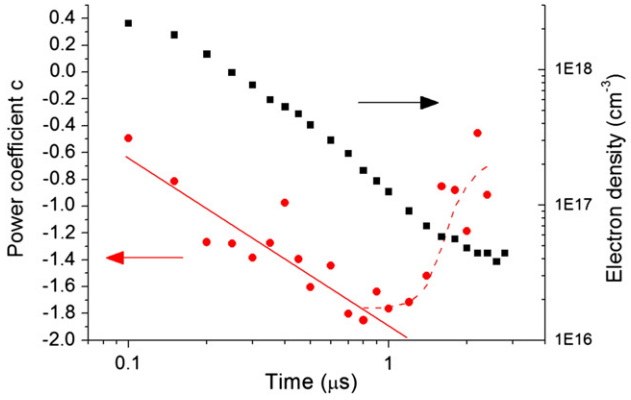

Fig. 9. Electron density (black squares) and coefficient c of power law $n_e \propto t^c$ (red circles) vs. delay time calculated from data by Barthelemy et al. [68].

ionization rate is very low ($kT_e \ll E_{ion}$) and very sensitive to temperature changes and cannot fully balance the recombination rate. Moreover, the recombination character can be reinforced by the increase of radiative recombination with the fall of plasma temperature that to some extent balances the decrease of 3-body recombination rate [10]. Thus, the recombination character of the plasma in this stage, given by the sum of 2nd and 3rd terms in Eq. (18), can be significant, depending on the atomic system and on the value of the ionization energy. We note that non-metals are expected to be more recombinant than metals because of the greater ionization energy, and then are again more prone to non-LTE effects. To conclude, in the quasi-isothermal phase, we expect that the 1st term in Eq. (18) decreases while the sum of 2nd and 3rd terms can increase, depending on the plasma composition, so that the LTE attainment should be checked case by case.

Many papers in the last years tackled the issue of possible deviations from LTE due to the transient character of the LIBS plasmas. Most of them investigated the issue by comparing the experimentally measured ionization and excitation temperatures at different times of plasma evolution [68–70] or, which is the same, by comparing the l.h.s. (named the ionization reaction quotient) and r.h.s. (i.e. the equilibrium ratio) of the Saha equation reported in Eq. (10) [67]. Their results, usually obtained by spatially-integrated measurements, show a significant discrepancy between T_{exc} and T_{ion} at early times of plasma life while the two values tend to converge at times of the order of a few μs. All these works conclude that LTE is violated in the earlier phase of plasma evolution because of the short timescales of plasma decay during the expansion; differently, it is reported that LTE is likely to occur in the second phase because plasma confinement results in much longer decay timescales. In a detailed work, however, Aguilera et al. [97] showed that Abel-inverted spatial-resolved measurements lead to comparable values of T_{exc} and T_{ion} while spatial integrated measurements produce a significant discrepancy of these values, since neutral and ionized species are differently distributed into the plasma plume. Hence, Aguilera et al. cast doubts on the validity of the method described above for checking LTE, when it relies upon spatially-integrated measurements. Following their view, the approaching of T_{exc} and T_{ion} values at late times could be caused by the progressive homogenization of the plasma [119]. Other authors explained this discrepancy by hypothesizing a non-equilibrium due to the effects of radiative recombination or by the inadequacy of the Boltzmann plot to quantify the population of highly-excited states of neutral species [10,83].

Recently, Merten et al. [76] investigated the occurrence of LTE in transient plasmas by comparing the timescale of plasma decay with the relaxation time to LTE, calculated according to Eq. (13), at different times of plasma evolution. They carried out time-resolved measurements of micro-LIBS plasmas induced by a microchip laser (λ = 532 nm, τ = 0.5 ns) on aluminum target in air, argon and helium gases. Although the experimental conditions utilized by Merten et al. are markedly different from those typical of LIBS measurements (e.g. the lifetime of their microplasmas is of the order of only 100 ns), it is however worth summarizing their results, which significantly differ from those reported by the previous literature. In fact, they found that the second criterion of LTE., i.e. Eq. (11), is fulfilled in air and in argon gases at short times of evolution (respectively $t < 25$ ns and $t < 40$ ns) but not at longer times while the criterion is never fulfilled in helium. Using the same approach we compare in Fig. 10 the timescale of plasma decay and the relaxation times of different neutral species calculated at different evolution times. The data were again obtained by rearranging the results of Barthelemy et al. [68] and of El Rabii et al. [99], the same utilized in Fig. 7. Fig. 10a and b shows that at early times, all the species exhibit relaxation times much shorter than the decay timescale of the plasma. This is similar to what happens in vacuum and agrees with the fact that at the end of the laser pulse or immediately after it, the plasma enters in LTE leaving its ionizing character and maintains this state until the electron density becomes so low that it is no more able to keep the system in LTE. Therefore, this approach suggests that despite the rapid expansion following the breakdown, at early times the electron density is large enough for ensuring LTE, which is in contrast with the conclusions drawn in Refs. [68–71]. With elapsing the time, the relaxation times of all the species increase due to the fall of electron density and temperature, so that LTE assumption can become critical at later times of evolution. At these times, however, the stopping of the plume can strongly facilitate the maintaining of LTE. The transitions of plasma decay timescale at ~2 μs and ~0.8 μs in Fig. 10a and b, respectively, denote the effect of plasma confinement and suggest that the reduction of the 1st term in Eq. (18) is predominant onto the (eventual) increase of the sum of 2nd and 3rd terms. According to the picture delineated in Ref. [17], metal species more easily remain in LTE than non-metal species, as clearly shown in Fig. 10, because of the smaller energy gap between the ground and the resonance level. From Fig. 10b it is evident that the effect of plasma confinement is significant but not sufficient to grant the LTE attainment for neutral nitrogen. This agrees with the results of Cristoforetti et al. [25] and Ma et al. [75], which both show that the transient criterion is satisfied for metal species but not for species deriving from the background gas (which are respectively air and argon). The validity of this approach, utilizing the transient criterion, seems confirmed in Ref. [25], where a spatial-resolved detection apparatus is used, by the finding that $T_{ion} = T_{exc}$ for aluminum, while $T_{ion} > T_{exc}$ for nitrogen, which testifies its recombination character. Similarly, Boker and Bruggemann [86], analyzing laser-induced plasmas induced in air at 0.8–1.6 MPa pressures by a ns Nd:YAG laser pulse, observed deviations from LTE at times larger than 3.5 μs, where deviations seem to increase with the delay time.

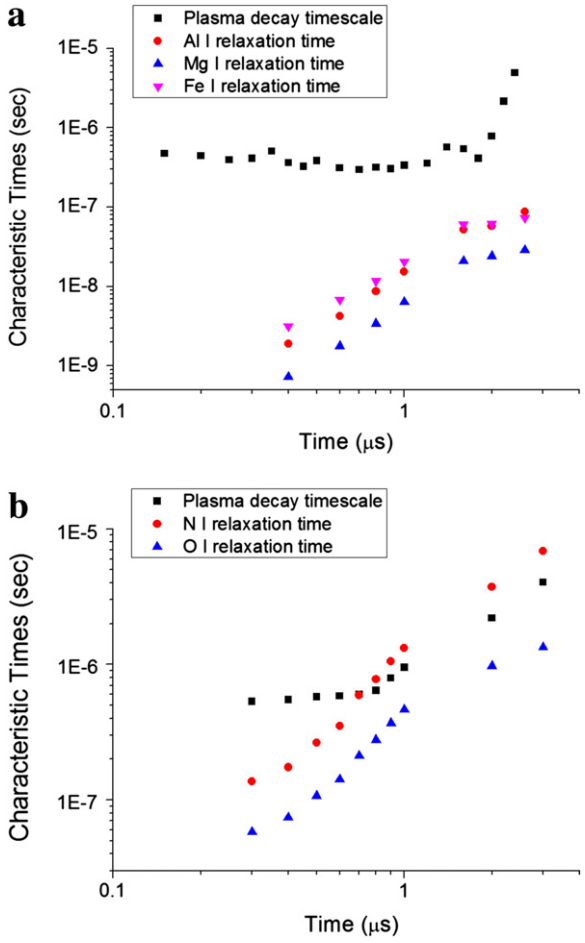

Fig. 10. Characteristic time of plasma decay (black squares) and the relaxation times to LTE of different neutral species, calculated at different evolution times, from the works of Barthelemy et al. [68] (a) and El Rabii et al. [99] (b).

In Ref. [99], from which the data in Fig. 10b are taken, the authors theoretically investigated the LTE assumption by modeling the plume expansion according to the point strong explosion solution. The comparison of theoretical results, based on LTE fulfillment, and the experimental results shows a substantial agreement except that at the longest delay times ($t > \sim 1$ μs), which is explained by the authors by the unreliability of blast wave model at large delay times. The trends of relaxation times plotted in Fig. 10b show that such discrepancy could also be produced by the recombination character of nitrogen at such times.

We want to remark that deviations from LTE due to transient effects for times shorter than 400 ns in Fig. 10a, for example produced by the radiative recombination of Al^{2+} ions, could be possible and should be taken in consideration; more in general, the recombination of multiply-ionized species at early times could constitute a cause of deviation from LTE.

It is also worth noticing that in a multi-element plasma it may happen that only some elements are in LTE; in case of experiments carried on at atmospheric pressure, it often occurs that the plasma is dominated by the background species, which therefore drive its evolution [25]. Similarly to what is found in Ref. [25], Hermann et al. [120] showed that metal-target atoms are in LTE, despite the background gas (in this case helium) is significantly recombining.

The more critical situation for LTE at long times agrees also with the fact that during the evolution, the plasma becomes more and more recombinant with elapsing the time, as shown by the trend of the power coefficient c in Fig. 9. It is also worth to remark that deviations from LTE at late times (10^{-6}–10^{-5} s) can be also produced by the onset of radiative recombination of singly-ionized species, by the spontaneous emission from metastable low-lying levels and by inelastic and superelastic electron collisions, as shown in Ref. [10].

In conclusion, the modeling and the experimental results investigating on LTE deviations due to the transient character of the plasma, show some discrepancy about the times which are more favorable for the establishment of LTE. In fact, basic considerations about typical times of expansion and recombination suggest that early times are more suitable for LTE than late times, even if gas confinement can strongly help to maintain LTE conditions in the latter phase of plasma life. This however contradicts some experimental results. New experiments utilizing spatially-resolved measurements and focused on the investigation of LIBS plasmas at early times, appear necessary to give a more accepted and decisive picture of the phenomenon.

4.4. Diffusion processes and LTE

The issue of particle diffusion in thermal plasmas, such as arc discharge plasmas, ICP torches or flames, was investigated in some papers [29,33,121], aimed at determining the diffusion coefficients of plasma species, at detecting spatial variation of chemical elements concentration (i.e. the 'demixing' effect) or at studying the deviations from LTE. Snyder et al. [29] studied the diffusion processes in an argon–hydrogen plasma induced by an arc discharge at atmospheric pressure by using a two-photon laser-induced fluorescence; they found a spatial profile of hydrogen not compatible with the profiles calculated by assuming the thermodynamic equilibrium and explained this result by demonstrating that the diffusion rate of atomic hydrogen is larger than its recombination rate.

The diffusion in LIBS plasmas is still almost unexplored and just a small number of paper reports on its effects on the establishment of LTE. To our knowledge, no paper in the literature tackled this phenomenon in detail. This lack is probably due to the complexity of the issue, which, if treated theoretically, would require the calculation of a large number of collision cross sections for a multi-element plasma. On the other hand, an experimental determination of the diffusion coefficients is complicated by the inhomogeneity and transient character of the plasma. Experimental measurements of diffusion coefficients in LIBS plasmas were carried out by Hohreiter and Hahn [122] and Diwakar et al. [123] by using ICCD imaging of atomic emission. The coefficient for hydrogen measured by Diwakar et al. was in good agreement with the theoretical value and at least an order of magnitude higher than the coefficient for calcium. By considering the obtained coefficient for hydrogen and typical plasma parameters, they remarked that the diffusion length of hydrogen during the thermal relaxation time is significantly larger than the typical plasma scale-length, implying the presence of deviations from LTE. Other papers where the effects of diffusion on LTE were discussed are the works of Cristoforetti et al. [17,25] and Ma et al. [75], where the criterion in Eq. (14) is checked by utilizing experimental results. In Ref. [17], the data obtained in Ref. [97] were utilized, where the plasma was induced by a ns Nd:YAG laser on a Fe–Ni target in air at atmospheric pressure. By considering the temporal window 3–3.5 μs, it was observed that the criterion is easily fulfilled for metal species (Cu, Fe, Ni), while it is not for non-metals (O, H). In Ref. [25], where an Al plasma induced in air by a ns Nd:YAG laser is observed at the delay time 1–2 μs, the criterion is fulfilled for both metal and non-metals.

In the paper of Ma et al. [75] the plasma was induced by a ns Nd:YAG laser on an Al target in Ar gas and the criterion was checked in the time windows 600–800 ns and 3–4 μs. While at the shorter delay time the criterion was fulfilled for both Al and Ar species, at the longest one, the Ar species did not fulfill it, similarly to what found in Ref. [17].

Here, we present other examples which reinforce the picture given by the results reported above. In Fig. 11 the diffusion length of plasma species vs. the delay time in three different cases are reported. The blue triangles and red circles data are rearranged from Ref. [68] and refer to Al I and Mg I species in an Al plasma. The diffusion length of Al atoms, which is the matrix element, was calculated by utilizing Eq. (15), while that of Mg, which is a trace element, was calculated by means of Eq. (15b). In both cases, we assumed $T_e = T_H$. The comparison between Al and Mg confirms that the diffusion length of neutral atoms of trace elements is higher than that of matrix elements, as reported in Ref. [13], and suggests that trace elements are more easily affected by non-LTE effects.

The diffusion lengths of nitrogen atoms are calculated from the data in Ref. [99], and therefore apply to different experimental conditions. However, the values appear comparable to those calculated in

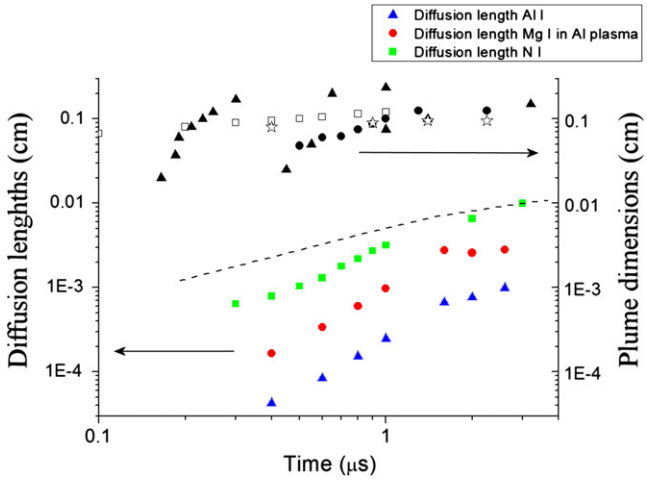

Fig. 11. Comparison of typical diffusion lengths of atomic species with plume dimensions. Blue triangles: Al I species in an Al plasma from Ref. [68]. Red circles: Mg I species in an Al plasma from Ref. [68]. Green squares: N I species in an air plasma from Ref. [68]. Black symbols represent the plume position measured in different experiments at atmospheric pressure: circles from Ref. [117] (Ti target in air), empty squares from Ref. [124] (Cu target in Ar), triangles from Ref. [114] (steel target in air), and empty stars from Ref. [113] (plasma in air). The dashed line represents the limit above which diffusion effects can produce LTE violation.

Refs. [25,75] an thus confirm that non-metals are more prone to LTE deviations than metals.

By looking at the figure, it is also evident that the diffusion length increases with the time delay, because of the reduction of the density and of the growth of the equilibration times.

In order to compare the diffusion lengths with typical plasma dimensions, we reported in Fig. 11 values of LIBS plume dimensions, as measured in different experiments [113,114,117,124]. Despite the variety of experimental conditions – where the irradiance, the target composition, the focusing conditions and the background composition are different – the dimensions of the plume do not vary significantly and are within a factor of 2-5, depending on the delay –time. By using these data, we plotted in the graph the limit for which the criterion is satisfied, indicated by the dashed line in the figure. The limit suggests that deviations from LTE more easily occur at late delay times, i.e. after a few microseconds, and for non-metals species. This result agrees with those presented in Refs. [17,25,75].

From the above considerations, it is also obvious that the situation becomes particularly critical in cases where non-metals are present in the plasma as traces, as for example for the LIBS analysis of soils.

We want here to emphasize that the above results and conclusions have been drawn by utilizing approximated values of the diffusion coefficients, calculated by means of Eqs. (15), (15b), that can be largely inexact. In order to confirm the picture delineated above, it appears crucial to intensify the research toward the experimental measurements of diffusion coefficients in LIBS plasmas as well as to the theoretical calculation of coefficients in multi-element plasmas.

5. Conclusions

In this work, we have outlined the general framework describing the population of energy states in atomic/ionic systems in laser-induced plasmas. Beside a quick theoretical overview of the main aspects, the most frequent scenarios occurring in the laboratory were presented, referring to the relevant literature. The main differences in the population distribution in the atomic energy system driven by the duration of the laser pulse, the laser irradiance, the background gas environment, the target composition and the observation time of the plasma were discussed, tracing the effects of the different experimental parameters.

Plasmas produced by intense and ultra-intense laser pulses were quickly described with the purpose of giving a general, even if incomplete, overview. Research about hot plasmas is mainly focused to obtain intense sources of X-rays, γ-rays, electron or proton beams, to achieve experimental conditions suitable for the inertial confinement fusion or to mimic in the laboratory processes of astrophysical interest. The typical n_e–T_e values imply that collisional–radiative models need to be utilized, since n_e is too high to produce coronal equilibrium and too low to fulfill the LTE condition. The observation time of the plasma is usually that of laser-plasma interaction or immediately successive, where non-steady state effects can be significant. This is particularly true in the case of ultra-short, ultra-intense laser pulses. For this reason, CR models should be time-dependent and coupled to hydrodynamic codes describing plasma expansion.

Particular emphasis was given to the occurrence of local thermodynamic equilibrium in LIBS plasmas, which appears to be a key issue for the beneficial utilization of the technique. The issue is particularly crucial for methodologies, aimed at determining quantitatively the composition of the target, that rely on the so called calibration-free approach.

The main causes of deviation from LTE in LIBS plasmas – namely radiative, transient and diffusive processes – were discussed, both from a theoretical point of view and by referring to experimental results present in the literature. The theoretical investigation, based on the simplified approach of the LTE criteria and not on the utilization of complete kinetic codes, accounted only for the dominant processes in the plasma and is therefore subjected to some uncertainties. Nevertheless, it allows an intuitive comprehension of the phenomena which play a role that appears to us fundamental. Results of such analysis, making use of experimental results present in the literature, converge to the picture that a LIBS plasma enters into LTE near the end of the laser pulse and maintains this status for a certain time, depending on the background pressure and on the plasma composition. In this temporal range, which could be of the order of a microsecond, the electron density is in fact large enough to ensure the predominance of collisional processes in level population, short times of relaxation to the equilibrium and reduced diffusion lengths of particles. This picture, however, could be significantly modified if the radiative recombination of multiply-charged ions at early times would play an important role.

Earlier times can be dominated by ionization, in particular in case of fs laser pulse, while successive times could be dominated by radiative effects (spontaneous decay and radiative recombination), by the strong recombination and diffusive effects. The plasma confinement occurring at a later stage of evolution can help the system to maintain in LTE, but its effect contrasts with the increase of relaxation times with the delay time; therefore, this point needs to be investigated.

LIBS measurements performed in vacuum or in low pressure environments are especially critical because of the rapid fall of electron density, which produces a faster exit from LTE. The quantitative analysis of non-metal species in LIPs appears also insidious, since their large energy gap from the ground to the first excited level leads to more restrictive conditions for the electron density needed to ensure the validity of the steady-state approximation and the predominance of collisional processes in determining level population. The same applies to the analysis of trace elements because of their large diffusion lengths in the plasma.

The picture delineated above is in a striking contradiction with the results obtained in a certain number of experimental works based on space-integrated measurements. In those works, mentioned in Section 4, different values of excitation and ionization temperatures up to times of the order of a microsecond were obtained, which was interpreted as an indication of the non-steady-state condition of the plasma in this time lag. To resolve this controversy, new experimental measurements utilizing space- and time-resolved apparatus appear necessary.

We finally want to emphasize that, while in the community working on hot and dense plasmas the modeling approach is well established, and commercial and free codes are available and became popular, in case of LIBS plasmas this approach is rare and deficient. This is probably caused also by the hard task of modeling plasma breakdown and plume expansion in a background gas at atmospheric pressure. Nevertheless, theoretical investigation of transient effects, i.e. kinetic modeling, sided by the utilization of hydrodynamic codes appears necessary as well as the modeling of particle diffusion in multi-element plasmas. The discussion of the latter issue is at the moment completely absent in the LIBS literature.

References

[1] D.R. Bates, A.E. Kingston, R.W.P. McWhirter, Recombination between electrons and atomic ions. I. Optically thin plasmas, Proc. R. Soc. Lond. A 267 (1962) 297–312.
[2] D.R. Bates, A.E. Kingston, R.W.P. McWhirter, Recombination between electrons and atomic ions. II. Optically thick plasmas, Proc. R. Soc. Lond. A 270 (1962) 155–167.
[3] B. van der Sijde, J.A.M. van der Mullen, Temperature determination in non-LTE plasmas, J. Quant. Spectrosc. Radiat. Transf. 44 (1990) 39–46.
[4] T. Fujimoto, Plasma spectroscopy, Clarendon Press, Oxford, 2004.
[5] J.A.M. van der Mullen, Excitation equilibria in plasmas; a classification, Phys. Rep. 191 (1990) 109–220.
[6] L. Spitzer, Physics of Fully Ionised Gases, 2nd edn Interscience, New York, 1962.
[7] D. Li, New Coulomb logarithm and its effects on the Fokker–Planck equation, relaxation times and cross-field transport in fusion plasmas, Nucl. Fusion 41 (2001) 631–635.
[8] J.A.M. van der Mullen, On the atomic state distribution function in inductively coupled plasmas — II. The stage of local thermal equilibrium and its validity region, Spectrochim. Acta Part B 45 (1990) 1–13.
[9] M. Capitelli, F. Capitelli, A. Eletskii, Non-equilibrium and equilibrium problems in laser-induced plasmas, Spectrochim. Acta Part B 55 (2000) 559–574.
[10] L.D. Pietanza, G. Colonna, A. De Giacomo, M. Capitelli, Kinetic processes for laser induced plasma diagnostic: a collisional–radiative model approach, Spectrochim. Acta Part B 65 (2010) 616–626.

[11] H.R. Griem, Plasma Spectroscopy, McGraw-Hill Inc., New York, 1964.
[12] H.R. Griem, Validity of local thermal equilibrium in plasma spectroscopy, Phys. Rev. 131 (1963) 1170–1176.
[13] H.W. Drawin, Validity conditions for local thermodynamic equilibrium, Z. Phys. 228 (1969) 99–119.
[14] R. Wilson, The spectroscopy on non-thermal plasmas, J. Quant. Spectrosc. Radiat. Transf. 2 (1962) 477–490.
[15] J.D. Hey, Criteria for local thermal equilibrium in non-hydrogenic plasmas, J. Quant. Spectrosc. Radiat. Transf. 16 (1976) 69–75.
[16] R.W.P. McWhirter, in: R.H. Huddlestone, S.L. Leonard (Eds.), Plasma diagnostic techniques, Academic Press, New York, 1965, pp. 201–264.
[17] G. Cristoforetti, A. De Giacomo, M. Dell'Aglio, S. Legnaioli, E. Tognoni, V. Palleschi, N. Omenetto, Local thermodynamic equilibrium in laser-induced breakdown spectroscopy: beyond the McWhirter criterion, Spectrochim. Acta Part B 65 (2010) 86–95.
[18] H. Van Regemorter, Rate of collisional excitation in stellar atmospheres, Astrophys. J. 136 (1962) 906–915.
[19] R.C. Elton, in: H.R. Griem, R.H. Lovberg (Eds.), Methods of Experimental Physics, vol. 9 Part A, Academic Press, New York, 1970.
[20] J.D. Hey, C.C. Chu, J.P.S. Rash, Partial local thermal equilibrium in a low-temperature hydrogen plasma, J. Quant. Spectrosc. Radiat. Transf. 62 (1999) 371–387.
[21] M. Inokuti, Inelastic collisions of fast charged particles with atoms and molecules — the Bethe theory revisited, Rev. Mod. Phys. 43 (1971) 297–347.
[22] R.v.d.R Woolley, C.W. Allen, The coronal emission spectrum, Mon. Not. R. Astron. Soc. 108 (1948) 292–305.
[23] S. Byron, R.C. Stabler, P.I. Bortz, Electron–Ion recombination by collisional and radiative processes, Phys. Rev. Lett. 8 (1962) 376–379.
[24] J.G. Baker, D.H. Menzel, Physical processes in gaseous nebulae III. The Balmer decrement, Astrophys. J. 88 (1938) 52.
[25] G. Cristoforetti, G. Lorenzetti, S. Legnaioli, V. Palleschi, Investigation on the role of air in the dynamical evolution and thermodynamic state of a laser-induced aluminium plasma by spatial- and time-resolved spectroscopy, Spectrochim. Acta Part B 65 (2010) 787–796.
[26] T. Fujimoto, R.W.P. McWhirter, Validity criteria for local thermodynamic equilibrium in plasma spectroscopy, Phys. Rev. A 42 (1990) 6588–6601.
[27] W. Engelhardt, Establishment of partial local thermal equilibrium in transient and inhomogeneous plasmas, Phys. Fluids 16 (1973) 217–220.
[28] W.A. Cilliers, J.D. Hey, J.P.S. Rash, Thermal equilibrium criteria in a nitrogen plasma, J. Quant. Spectrosc. Radiat. Transf. 15 (1975) 963–978(erratum 16 (1976) 627).
[29] S.C. Snyder, A.B. Murphy, D.L. Hofeldt, L.D. Reynolds, Diffusion of atomic hydrogen in an atmospheric-pressure free-burning arc discharge, Phys. Rev. E. 52 (1995) 2999–3009.
[30] J.O. Hirschfelder, C.F. Curtiss, R.B. Bird, Molecular Theory of Gases and Liquids, 2nd ed. Wiley, New York, 1964.
[31] S. Chapman, T.G. Cowling, The mathematical theory of non-uniform gases: an account of the kinetic theory of viscosity, Thermal Conduction and Diffusion in Gases, Cambridge University Press, 1970.
[32] A.B. Murphy, Diffusion in equilibrium mixtures of ionized gases, Phys. Rev. E. 48 (1993) 3594–3603.
[33] A.B. Murphy, Modelling and diagnostics of plasma chemical processes in mixed-gas arcs, Pure Appl. Chem. 68 (1996) 1137–1142.
[34] A.B. Murphy, Transport coefficients of hydrogen and argon–hydrogen plasmas, Plasma Chem. Plasma Process. 20 (2000) 279–297.
[35] A.B. Murphy, Thermal plasmas in gas mixtures, J. Phys. D. Appl. Phys. 34 (2001) R151–R173.
[36] F.F. Chen, Introduction to plasma physics and controlled fusion, Plasma Physics, vol.1, Springer, 2006.
[37] N.A. Krall, A.W. Trivelpiece, Principles of Plasma Physics, San Francisco Press Inc., 1986
[38] W. Kruer, The Physics of Laser Plasma Interactions, Addison-Wesley, 1988.
[39] D.W. Forslund, J.M. Kindel, K. Lee, Theory of hot-electron spectra at high laser intensity, Phys. Rev. Lett. 39 (1977) 284–288.
[40] L.A. Gizzi, D. Batani, V. Biancalana, A. Giulietti, D. Giulietti, X-ray emission from thin-foil laser produced plasmas, Laser and Particle Beams, 101992. 65–74.
[41] M.H. Key, in: A. Rubenchick, S. Witkowsky (Eds.), Handbook of Plasma Physics, vol.3, North-Holland, 1991, pp. 575–611.
[42] R.W. Lee, J.T. Larsen, A time-dependent model for plasma spectroscopy of K-shell emitters, J. Quant. Spectrosc. Radiat. Transf. 56 (1996) 535–556.
[43] H.-K. Chung, M.H. Chen, W.L. Morgan, Y. Ralchenko, R.W. Lee, FLYCHK: generalized population kinetics and spectral model for rapid spectroscopic analysis for all elements, High Energy Density Physics, 12005. 3–12.
[44] A. Bar-Shalom, M. Klapisch, J. Oreg, HULLAC, an integrated computer package for atomic processes in plasmas, J. Quant. Spectrosc. Radiat. Transf. 71 (2001) 169–188.
[45] J.P. Christiansen, D.E.T.F. Ashby, K.V. Roberts, MEDUSA a one-dimensional laser fusion code, Comput. Phys. Commun. 7 (1974) 271–287.
[46] G.J. Pert, Two-dimensional hydrodynamic models of laser-produced plasmas, J. Plasma Phys. 41 (1989) 263.
[47] R. Ramis, R. Schmalz, J. Meyer-Ter-Vehn, MULTI, a computer code for one-dimensional multigroup radiation hydrodynamics, Comput. Phys. Commun. 49 (1988) 475–505.
[48] G.P. Gupta, B.K. Sinha, Effect of ionization and recombination coefficients on the charge-state distribution of ions in laser-produced aluminum plasmas, Phys. Rev. E. 56 (1997) 2104–2111.
[49] E. Louzon, Y. Franka, E. Raicher, P. Mandelbaum, A. Feigel, I. Levy, G. Hurvitz, Y. Ehrlich, M. Fraenkel, S. Maman, A. Zigler, Z. Henis, Diagnostics of dielectronic processes in laser produced samarium plasma, High Energy Density Physics, 82012. 81–87.
[50] W. Lotz, An empirical formula for the electron-impact ionization cross-section, Z. Phys. 206 (1967) 205–211.
[51] L.A. Gizzi, C.A. Cecchetti, M. Galimberti, A. Giulietti, D. Giulietti, L. Labate, S. Laville, P. Tomassini, Transient ionization in plasmas produced by point-like irradiation of solid Al targets, Phys. Plasmas 10 (2003) 4601–4604.
[52] L. Labate, C.A. Cecchetti, M. Galimberti, A. Giulietti, D. Giulietti, L.A. Gizzi, Detailed characterization of the early X-ray emission of a plasma produced by point-like laser irradiation of solid Al targets, Phys. Plasmas 12 (2005) 083101.
[53] D. Strickland, G. Mourou, Compression of amplified chirped optical pulses, Opt. Commun. 56 (1985) 219–221.
[54] L.A. Gizzi, S. Betti, M. Galimberti, A. Giulietti, D. Giulietti, L. Labate, T. Levato, P. Tomassini, P. Monot, T. Ceccotti, P. De Oliveira, Ph. Martin, Tracking propagation of ultrashort intense laser pulses in gases via probing of ionization, Phys. Rev. E. 79 (2009) 056405.
[55] F. Brunel, Not-so-resonant, resonant absorption, Phys. Rev. Lett. 59 (1987) 52–55.
[56] L. Labate, M. Galimberti, A. Giulietti, D. Giulietti, P. Köster, P. Tomassini, L.A. Gizzi, Study of forward accelerated fast electrons in ultrashort Ti Kalpha sources, Appl. Phys. B 86 (2007) 229–233.
[57] M. Tabak, J. Hammer, M.E. Glinsky, W.L. Kruer, S.C. Wilks, J. Woodworth, E.M. Campbell, M.D. Perry, R.J. Mason, Ignition and high gain with ultrapowerful lasers, Phys. Plasmas 1 (1994) 1626–1634.
[58] S.C. Wilks, W.L. Kruer, M. Tabak, A.B. Langdon, Absorption of ultra-intense laser pulses, Phys. Rev. Lett. 69 (1992) 1383–1386.
[59] F.N. Beg, A.R. Bell, A.E. Dangor, C.N. Danson, A.P. Fews, M.E. Glinsky, B.A. Hammel, P. Lee, P.A. Norreys, M. Tatarakis, A study of picosecond laser–solid interactions up to 1019 W cm^{-2}, Phys. Plasmas 4 (1997) 447–457.
[60] M. Protopapas, C.H. Keitel, P.L. Knight, Atomic physics with super-high intensity lasers, Rep. Prog. Phys. 60 (1997) 389–486.
[61] G.L. Yudin, M.Y. Ivanov, Nonadiabatic tunnel ionization: looking inside a laser cycle, Phys. Rev. A 64 (2001) 013409.
[62] H. Alfven, On the motion of cosmic rays in interstellar space, Phys. Rev. 55 (1939) 425–429.
[63] B.A. Remington, R.P. Drake, D.D. Ryutov, Experimental astrophysics with high power lasers and *Z* pinches, Rev. Mod. Phys. 78 (2006) 755–807.
[64] G. Cristoforetti, M.P. Anania, A.Y. Faenov, A. Giulietti, D. Giulietti, S.B. Hansen, P. Koester, L. Labate, T. Levato, T.A. Pikuz, L.A. Gizzi, Spatially resolved analysis of Kα X-ray emission from plasmas induced by a femtosecond weakly relativistic laser pulse at various polarizations, Phys. Rev. E. 87 (2013) 023103.
[65] E. Tognoni, G. Cristoforetti, S. Legnaioli, V. Palleschi, Calibration-free laser-induced breakdown spectroscopy: state of the art, Spectrochim. Acta Part B 65 (2010) 1–14.
[66] H.-Y. Moon, B.W. Smith, N. Omenetto, Temporal behavior of line-to-continuum ratios and ion fractions as a means of assessing thermodynamic equilibrium in laser-induced breakdown spectroscopy, Chem. Phys. 398 (2012) 221–227.
[67] A. De Giacomo, M. Dell'Aglio, R. Gaudiuso, A. Santagata, G.S. Senesi, M. Rossi, M.R. Ghiara, F. Capitelli, O. De Pascale, A laser induced breakdown spectroscopy application based on local thermodynamic equilibrium assumption for the elemental analysis of alexandrite gemstone and copper-based alloys, Chem. Phys. 398 (2012) 233–238.
[68] O. Barthelemy, J. Margot, S. Laville, F. Vidal, M. Chaker, B. Le Drogoff, T.W. Johnston, M. Sabsabi, Investigation of the state of local thermodynamic equilibrium of a laser-produced aluminium plasma, Appl. Spectrosc. 59 (2005) 529–536.
[69] M. Milan, J.J. Laserna, Diagnostics of silicon plasmas produced by visible nanosecond laser ablation, Spectrochim. Acta Part B 56 (2001) 275–288.
[70] B. Le Drogoff, J. Margot, M. Chaker, M. Sabsabi, O. Barthelemy, T.W. Johnston, S. Laville, F. Vidal, Y. von Kaenel, Temporal characterization of femtosecond laser pulses induced plasma for spectrochemical analysis of aluminum alloys, Spectrochim. Acta Part B 56 (2001) 987–1002.
[71] J.B. Simeonsson, A.W. Miziolek, Time-resolved emission studies of ArF-laser-produced microplasmas, Appl. Opt. 32 (1993) 939–947.
[72] M. Thiyagarajan, J. Scharer, Experimental investigation of ultraviolet laser induced plasma density and temperature evolution in air, J. Appl. Phys. 104 (2008) 013303.
[73] A.H. Galmed, M.A. Harith, Temporal follow up of the LTE conditions in aluminum laser induced plasma at different laser energies, Appl. Phys. B 91 (2008) 651–660.
[74] A. Alonso-Medina, Measured Stark widths of several spectral lines of Pb III, Spectrochim. Acta Part B 66 (2011) 439–443.
[75] Q.L. Ma, V. Motto-Ros, W.Q. Lei, M. Boueri, X.S. Bai, L.J. Zheng, H.P. Zeng, J. Yu, Temporal and spatial dynamics of laser-induced aluminum plasma in argon background at atmospheric pressure: Interplay with the ambient gas, Spectrochim. Acta Part B 65 (2010) 896–907.
[76] J.A. Merten, B.W. Smith, N. Omenetto, Local thermodynamic equilibrium considerations in powerchip laser-induced plasmas, Spectrochim. Acta Part B 83–84 (2013) 50–55.
[77] I.B. Gornushkin, U. Panne, Radiative models of laser-induced plasma and pump-probe diagnostics relevant to laser-induced breakdown spectroscopy, Spectrochim. Acta Part B 65 (2010) 345–359.
[78] G.L. Payne, J.D. Perez, T.E. Sharp, B.A. Watson, Recombination effects in an expanding laser produced plasma, J. Appl. Phys. 49 (1978) 4688–4693.
[79] G. Colonna, L.D. Pietanza, M. Capitelli, Coupled solution of a time-dependent collisional–radiative model and Boltzmann equation for atomic hydrogen plasmas: possible implications with LIBS plasmas, Spectrochim. Acta Part B 56 (2001) 587–598.
[80] G. Travaillé, O. Peyrusse, B. Bousquet, L. Canioni, K. Michel-Le Pierres, S. Roy, Local thermodynamic equilibrium and related metrological issues involving collisional–radiative model in laser-induced aluminum plasmas, Spectrochim. Acta Part B 64 (2009) 931–937.

[81] V.I. Babushok, F.C. DeLucia Jr., P.J. Dagdigianc, A.W. Miziolek, Experimental and kinetic modeling study of the laser-induced breakdown spectroscopy plume from metallic lead in argon, Spectrochim. Acta Part B 60 (2005) 926–934.
[82] C.D. David, H. Weichel, Temperature of a laser heated carbon plasma, J. Appl. Phys. 40 (1969) 3674–3679.
[83] A. De Giacomo, R. Gaudiuso, M. Dell'Aglio, A. Santagata, The role of continuum radiation in laser induced plasma spectroscopy, Spectrochim. Acta Part B 65 (2010) 385–394.
[84] G.J. Bastiaans, R.A. Mangold, The calculation of electron density and temperature in Ar spectroscopic plasmas from continuum and line spectra, Spectrochim. Acta Part B 40 (1985) 885–892.
[85] P.D. Johnston, Measurement of LTE plasma temperatures below 10000 K, J. Phys. D. Appl. Phys. 3 (1970) 1999.
[86] D. Boker, D. Bruggemann, Temperature measurements in a decaying laser-induced plasma in air at elevated pressures, Spectrochim. Acta Part B 66 (2011) 28–38.
[87] R.E. Bentley, A departure from local thermodynamic equilibrium within a freely burning arc and asymmetrical Thomson electron features, J. Phys. D. Appl. Phys. 30 (1997) 2880–2886.
[88] M. Huang, G.M. Hieftje, Simultaneous measurement of spatially resolved electron temperatures, electron number densities and gas temperatures by laser light scattering from the ICP, Spectrochim. Acta Part B 44 (1989) 739–749.
[89] K. Dzierżęga, A. Mendys, B. Pokrzywka, W. Zawadzki, S. Pellerin, Simultaneous measurement of electron and heavy particle temperatures in He laser-induced plasma by Thomson and Rayleigh scattering, Appl. Phys. Lett. 102 (2013) 134108.
[90] C. Parigger, D.H. Plemmons, J.O. Hornkohl, J.W.L. Lewis, Spectroscopic temperature measurements in a decaying laser-induced plasma using the C_2 Swan system, J. Quant. Spectrosc. Radiat. Transf. 52 (1994) 707–711.
[91] D.A. Rusak, B.C. Castle, B.W. Smith, J.D. Winefordner, Excitational, vibrational, and rotational temperatures in Nd:YAG and XeC1 Laser-Induced Plasmas, Spectrochim. Acta Part B 52 (1997) 1929–1935.
[92] A. Czernichowski, Temperature evaluation from the partially resolved 391 nm N_2^+ band, J. Phys. D. Appl. Phys. 20 (1987) 559–564.
[93] C.O. Laux, T.G. Spence, C.H. Kruger, R.N. Zare, Optical diagnostics of atmospheric pressure air plasmas, Plasma Sources Sci. Technol. 12 (2003) 125–138.
[94] D.W. Hahn, N. Omenetto, Laser-induced breakdown spectroscopy (LIBS), part I: review of basic diagnostics and plasma–particle interactions: still-challenging issues within the analytical plasma community, Appl. Spectrosc. 64 (2010) 335A–366A.
[95] J. Jonkers, H.P.C. Vos, J.A.M. van der Mullen, E.A.H. Timmermans, On the atomic state densities of plasmas produced by the "torche à injection axiale", Spectrochim. Acta Part B 51 (1996) 457–465.
[96] G. Cristoforetti, E. Tognoni, Calculation of elemental columnar density from self-absorbed lines in laser-induced breakdown spectroscopy: a resource for quantitative analysis, Spectrochim. Acta Part B 79–80 (2013) 63–71.
[97] J.A. Aguilera, C. Aragon, Characterization of a laser-induced plasma by spatially resolved spectroscopy of neutral atom and ion emissions. Comparison of local and spatially integrated measurements, Spectrochim. Acta Part B 59 (2004) 1861–1876.
[98] L. Mercadier, J. Hermann, C. Grisolia, A. Semerok, Diagnostics of nonuniform plasmas for elemental analysis via laser-induced breakdown spectroscopy: demonstration on carbon-based materials, J. Anal. At. Spectrom. 28 (2013) 1446–1455.
[99] H. El-Rabii, S.B. Victorov, A.P. Yalin, Properties of an air plasma generated by ultraviolet nanosecond laser pulses, J. Phys. D. Appl. Phys. 42 (2009) 075203.
[100] J.A. Aguilera, C. Aragon, Temperature and electron density distributions of laser-induced plasmas generated with an iron sample at different ambient gas pressures, Appl. Surf. Sci. 197–198 (2002) 273–280.
[101] J.A. Aguilera, C. Aragón, G. Cristoforetti, E. Tognoni, Application of calibration-free laser-induced breakdown spectroscopy to radially resolved spectra from a copper-based alloy laser-induced plasma, Spectrochim. Acta Part B 64 (2009) 685–689.
[102] S. Amoruso, Modeling of UV pulsed-laser ablation of metallic targets, Appl. Phys. A 69 (1999) 323–332.
[103] W.L. Yip, E. Mothe, S. Beldjilali, J. Hermann, Accumulation of air in polymeric materials investigated by laser-induced breakdown spectroscopy, J. Appl. Phys. 111 (2012) 063108.
[104] X. Mao, S-b. Wen, R.E. Russo, Time resolved laser-induced plasma dynamics, Appl. Surf. Sci. 253 (2007) 6316–6321.
[105] Y. Ogino, N. Ohnishi, K. Sawada, Numerical study of laser-induced blast wave coupled with unsteady ionization processes, J. Phys. Conf. Ser. 112 (2008) 042019.
[106] Y. Ogino, N. Ohnishi, A collisional–radiative code for computing air plasma in high enthalpy flow, Shock Waves 21 (2011) 289–299.
[107] P.T. Rumsby, J.W.M. Paul, Temperature and density of an expanding laser produced plasma, Plasma Phys. 16 (1974) 247–260.
[108] I.V. Roudskoy, General features of highly charged ion generation in laser-produced plasmas, Laser Part. Beams, 141996. 369–384.
[109] M. Mattioli, Recombination processes during the expansion of a lase-produced plasma, Plasma Physics, 131971. 19–28.
[110] R.A. Burdt, Y. Ueno, Y. Tao, S. Yuspeh, M.S. Tillack, F. Najmabadi, Recombination effects during expansion into vacuum in laser produced Sn plasma, Appl. Phys. Lett. 97 (2010) 041502.
[111] L.I. Sedov, Similarity and Dimensional Methods in Mechanics, CRC Press, LCC, Moscow, 1993.
[112] K. Kagawa, K. Kawai, M. Tani, T. Kobayashi, XeCl excimer laser-induced shock wave plasma and its application to emission spectrochemical analysis, Appl. Spectrosc. 48 (1994) 198–205.
[113] G. Cristoforetti, S. Legnaioli, L. Pardini, V. Palleschi, A. Salvetti, E. Tognoni, Spectroscopic and shadowgraphic analysis of laser induced plasmas in the orthogonal double pulse pre-ablation configuration, Spectrochim. Acta Part B 61 (2006) 340–350.
[114] M. Corsi, G. Cristoforetti, M. Hidalgo, D. Iriarte, S. Legnaioli, V. Palleschi, A. Salvetti, E. Tognoni, Temporal and spatial evolution of a laser-induced plasma from a steel target, Appl. Spectrosc. 57 (2003) 715–721.
[115] S. Amoruso, A. Sambri, X. Wang, Plume expansion dynamics during laser ablation of manganates in oxygen atmosphere, Appl. Surf. Sci. 253 (2007) 7696–7701.
[116] M.M. Litvak, D.F. Edwards, Electron recombination in laser produced hydrogen plasma, J. Appl. Phys. 37 (1966) 4462–4474.
[117] A. De Giacomo, M. Dell'Aglio, D. Bruno, R. Gaudiuso, O. De Pascale, Experimental and theoretical comparison of single- and double-pulse LIBS on metallic samples, Spectrochim. Acta Part B 63 (2008) 805–816.
[118] A. De Giacomo, M. Dell'Aglio, R. Gaudiuso, G. Cristoforetti, S. Legnaioli, V. Palleschi, E. Tognoni, Spatial distribution of hydrogen and other emitters in aluminum laser-induced plasma in air and consequences on spatially integrated Laser-Induced Breakdown Spectroscopy measurements, Spectrochim. Acta Part B 63 (2008) 980–987.
[119] J.A. Aguilera, J. Bengoechea, C. Aragon, Curves of growth of spectral lines emitted by a laser-induced plasma: influence of the temporal evolution and spatial inhomogeneity of the plasma, Spectrochim. Acta Part B 58 (2003) 221–237.
[120] J. Hermann, C. Boulmer-Leborgne, B. Dubreuil, I.N. Mihailescu, Influence of irradiation conditions on plasma evolution in laser–surface interaction, I, Appl. Phys. 74 (1993) 3071–3079.
[121] A.B. Murphy, Demixing Due to frictional forces in an electric arc, Phys. Rev. Lett. 73 (1994) 1797–1800.
[122] V. Hohreiter, D.W. Hahn, Plasma–particle interactions in a laser-induced plasma: implications for laser-induced breakdown spectroscopy, Anal. Chem. 78 (2006) 1509–1514.
[123] P.K. Diwakar, S. Groh, K. Niemax, D.W. Hahn, Study of analyte dissociation and diffusion in laser-induced plasmas: implications for laser-induced breakdown spectroscopy, J. Anal. At. Spectrom. 25 (2010) 1921–1930.
[124] S.-B. Wen, X. Mao, R. Greif, R.E. Russo, Laser ablation induced vapor plume expansion into a background gas. II. Experimental analysis, J. Appl. Phys. 101 (2007) 023115.